International Journal of Engineering and Information Systems (IJEAIS)
ISSN: 2643-640X
Vol. 10 Issue 10, October - 2026, Pages: 220-243

Field Degradation, Soiling and Reliability of Photovoltaic Modules in the Hot-Humid and Hot-Arid Climates of Asia

Bahaaaldeen M. Abdulhadi[1]*

[1] Regional Director, E. A. Juffali & Brothers A/C, Mechanical & Electrical Co., Saudi Arabia.
Email: bahaa.alhadi@gmail.com
*Corresponding Author: Bahaaaldeen M. Abdulhadi
Email: bahaa.alhadi@gmail.com

Abstract*: Asia hosts most of the world's photovoltaic capacity, yet much of it operates in climates that standard qualification sequences were not designed to represent: the persistently wet and warm tropics of South and Southeast Asia, and the dusty, ultraviolet-intense deserts of the Gulf, the Thar and western China. This critical review appraises field and laboratory evidence on how modules degrade and soil in these two climate families and what the losses cost, keeping accelerated test results separate from observed field degradation. In the two Indian national surveys, crystalline silicon modules degraded on average at 1.33 to 1.47 percent per year, about 2.2 to 2.9 times the global median of 0.5 to 0.6 percent per year, with hot zones, small systems and rooftop mounting faring worst. Elsewhere the spread is wide: seven-year Singapore monitoring found 0.03 to 0.47 percent per year, whereas Thai and ten-year Singapore studies reported losses equivalent to several percent per year, so climate alone does not determine outcomes. Uncleaned modules in Qatar lost 43 to 50 percent of output within six to eight months. The review proposes the Climate-Resolved Reliability and Soiling Assessment (CRRSA) framework and demonstrates it with an illustrative calculation in which measured hot-zone degradation raises levelised cost by about 8 percent at a hot-humid site, while cleaning policy dominates at a hot-arid site. The framework is not yet validated.*

Keywords: photovoltaic reliability; field degradation rate; soiling; potential-induced degradation; hot-humid climate; hot-arid climate

1. Introduction

The geography of photovoltaic (PV) deployment has shifted towards Asia, and with it the climatic envelope in which modules must survive for twenty-five to thirty years. India, China, the Gulf Cooperation Council states, Pakistan and the members of the Association of Southeast Asian Nations are adding capacity in locations whose stresses differ from the temperate European and North American sites where most long-term reliability data were first collected. Two climate families dominate this expansion. The first is the hot-humid tropics, typified by coastal India, Bangladesh, Thailand, Malaysia, Singapore, Indonesia, Vietnam and the Philippines, where module temperatures are high, humidity rarely falls, dew forms most nights, and rain is frequent but irregular. The second is the hot-arid belt, which stretches from the Arabian Peninsula across southern Iran and Pakistan into the Thar Desert of north-western India and the deserts of western China. Here irradiance and ultraviolet (UV) dose are high, diurnal temperature swings are large, and airborne dust deposits on glass at rates that, in the Gulf studies reviewed, removed a large fraction of output within months (Ilse et al., 2019; Fares et al., 2021).

Global syntheses have established a reference point for long-term performance. The analytical review by Jordan and Kurtz (2013) and the later compendium of more than 11,000 degradation rates from nearly 200 studies in 40 countries placed the median for crystalline silicon at about 0.5 to 0.6 percent per year, with a mean of 0.8 to 0.9 percent per year (Jordan et al., 2016). A later study of 834 fielded modules of recent design in three climates reported a mean of 0.62 and a median of 0.58 percent per year (Theristis et al., 2023), while a 2025 meta-analysis of 610 observations from 80 studies returned a median of 0.94 percent per year and found that cell technology, mounting and methodological choices significantly influenced reported rates (Straub-Mück et al., 2025). These figures are frequently imported into Asian project finance models with little adjustment. The central question this review addresses is whether such imports are supported by the Asian field evidence, and, where they are not, what climate-resolved evidence should replace them.

The reasons to doubt transferability are physical. Most degradation chemistry is thermally activated, and moisture ingress through polymer backsheets and edge seals accelerates with both temperature and humidity (Segbefia et al., 2021). Potential-induced degradation (PID) depends on leakage currents that, at a given temperature, are several orders of magnitude larger at high relative humidity than at low humidity (Luo et al., 2017). UV-driven encapsulant browning and cell-level UV damage scale with dose, and high-efficiency cell architectures have proved more UV-sensitive than earlier designs in accelerated tests (Sinha et al., 2023). Soiling, finally, is not merely a cleaning problem: dust can cement onto glass under dew cycles and create non-uniform shading that drives

hot spots (Ilse et al., 2018b; Maghami et al., 2016). Each of these processes is plausibly more intense in at least one of the two Asian climate families than in the climates that shaped the qualification standards.

Earlier reviews have examined parts of this problem. Reviews of degradation and failure phenomena have catalogued mechanisms by module component without a climatic lens (Aghaei et al., 2022), reviews of humid-environment degradation have focused on technology performance under hot and humid conditions (Makhija & Bohra, 2023), and soiling reviews have concentrated on deposition physics or on individual regions such as the Gulf (Ilse et al., 2018a; Fares et al., 2021; Conceição et al., 2022). What is missing is an Asia-specific synthesis that places degradation, soiling and thermal derating in a single analytical frame, compares measured rates against global benchmarks with attention to method and sample size, and links technical findings to qualification practice and to the levelised cost of electricity (LCOE). This gap matters because the module technologies now shipping in volume, including bifacial glass-glass designs, tunnel-oxide passivated contact (TOPCon) cells and silicon heterojunction (HJT) cells, have failure signatures that the older field literature does not capture (Hacke et al., 2024; Pirot-Berson et al., 2024).

The stakes rise with scale. As cumulative deployment moves towards the terawatt level, reliability becomes a determinant of system cost, material demand and the credibility of decarbonisation pathways (Jordan et al., 2022). A simple compounding calculation shows the magnitude: raising annual degradation from 0.5 to 1.0 percent per year reduces the mean output of every 100 GW installed by about 6.8 percent over thirty years, equivalent to 6.8 GW of average output, and by about 13.6 percent in year thirty.

This review makes four contributions. First, it organises degradation modes by the climatic drivers that accelerate them, distinguishing accelerated laboratory evidence from field observation. Second, it compiles and compares field degradation rates and soiling losses measured at Asian sites, reporting sample size, technology generation, estimation method and uncertainty where available. Third, it evaluates the current editions of the IEC qualification standards against Asian conditions. Fourth, it proposes the Climate-Resolved Reliability and Soiling Assessment (CRRSA) framework and demonstrates it with an illustrative numerical application. The paper proceeds with the review approach (Section 2), degradation mechanisms (Section 3), field degradation rates (Section 4), soiling and cleaning (Section 5), thermal effects and testing (Section 6), economic consequences (Section 7), the CRRSA framework (Section 8) and a research agenda (Section 9), before concluding.

2. Review approach

This is a critical narrative review rather than a systematic review, and it does not follow the PRISMA protocol. The aim was to assemble the most informative evidence on climate-dependent PV reliability in Asia and to interrogate it. Searches were run in Scopus, Web of Science, ScienceDirect, Wiley Online Library, IEEE Xplore and Google Scholar between 2008 and 2026. The core search string combined a reliability block (“degradation rate” OR “field exposure” OR “potential-induced degradation” OR “encapsulant discolo*” OR delamination OR LeTID OR “UV-induced degradation” OR soiling OR dust OR “anti-soiling” OR “module temperature” OR “IEC 61215” OR LCOE) with a climate and place block (tropical OR humid OR desert OR arid OR the names of the Asian and Gulf countries listed in Section 1) and the term photovoltaic. Reference lists of the benchmark syntheses were then searched backwards (Jordan et al., 2016; Aghaei et al., 2022).

Inclusion required peer review (or, for one survey, publication by a national research institution), a quantitative result or a mechanistic explanation relevant to hot-humid or hot-arid conditions, and either an Asian site or a mechanism demonstrably active at Asian sites. Exclusion criteria were preprints, studies reporting only instantaneous efficiency without a temporal or soiling component, and duplicate reports of the same dataset. Earlier works were admitted only where they define methods still in use, such as module temperature models (Faiman, 2008; Skoplaki & Palyvos, 2009). The Indian national survey report was admitted because it is the largest climate-stratified field dataset in the region (National Centre for Photovoltaic Research and Education [NCPRE] & National Institute of Solar Energy [NISE], 2019). Studies from non-Asian deserts, such as Djibouti and Morocco, and one humid subtropical field test in Florida were retained as comparators where they isolate a mechanism more cleanly than Asian work does, and are labelled as such (Daher et al., 2022; Mehdi et al., 2023; Hacke et al., 2025). Qualification requirements were checked against the current IEC editions (International Electrotechnical Commission [IEC], 2021, 2025a).

Each item was coded by climate family, technology and generation, exposure duration, sample size and estimation method, and assigned an evidence-depth level using the three-level scale defined in Table 1. The scale grades how directly a result bears on long-term field behaviour in Asian climates; it does not grade study quality in an absolute sense.

Table 1. Evidence-depth scale used to appraise the reviewed studies.

Level	Definition	Typical examples
A	Field-measured, multi-site or large sample (more than about 50 modules)	Indian national surveys; multi-climate fleets
B	Single-site field measurement, accelerated laboratory test, or calibrated model	Science-park studies; damp heat, PID and UV tests
C	Descriptive, review-based or grey evidence without new measurement	Narrative reviews; techno-economic scenarios

Three limitations follow from the narrative design. Selection is judgement-based, so relevant studies in national-language journals may have been missed. No statistical pooling was attempted, because estimators, metrics and exposure periods differ too much for a defensible meta-analysis (Straub-Mück et al., 2025). Finally, many of the numbers compared below come from abstracts and full texts that report rates without uncertainty, which limits the precision of any cross-site comparison (Jordan & Kurtz, 2013).

3. Degradation mechanisms in hot-humid and hot-arid climates

Degradation in the field is rarely the action of a single mechanism. A module in a Thai or Malaysian array may simultaneously experience moisture ingress, acetic acid generation in its ethylene vinyl acetate (EVA) encapsulant, corrosion of its metallisation, and PID driven by night-time leakage across a wet glass surface. A module in Qatar or Rajasthan faces a different combination: high UV dose and module temperature that drive encapsulant browning, large daily thermal cycles that fatigue solder joints and interconnects, and dust that shades cells and, under dew, cements onto the glass. Reviews of failure phenomena organise these processes by component (Aghaei et al., 2022), while a global field synthesis found considerably higher degradation in hot, humid climates than in desert or moderate climates, with delamination and junction-box faults more frequent there (Jordan et al., 2017). As summarised in Table 2, the dominant modes differ between the two Asian climate families. Throughout this section, results from accelerated laboratory tests and from field exposure are identified as such, because the former establish susceptibility while only the latter establish observed rates.

Table 2. Principal degradation modes, their climatic accelerators, the climate family in which each is most consequential in Asia, and the type of supporting evidence.

Degradation mode	Main climatic drivers	Most exposed climate	Key evidence (type)
PID (shunting and polarisation)	Humidity, dew, temperature, system voltage	Hot-humid	Luo et al. (2017), review; Hacke et al. (2025), field with bias
Encapsulant discolouration	UV dose, temperature	Hot-arid and hot-humid	de Oliveira et al. (2018), review; NCPRE & NISE (2019), field
Delamination, moisture corrosion	Humidity, temperature, time of wetness	Hot-humid	Segbefia et al. (2021), review; Luo et al. (2021), field
Backsheet cracking and chalking	UV, thermal cycling, humidity	Hot-arid	Abdallah et al. (2024), field; Lyu et al. (2020), review
LeTID and UVID	Temperature, irradiance, UV	Both	Yeo et al. (2022), review; Sinha et al. (2023), laboratory
TOPCon and HJT degradation	Humidity, sodium, UV, bias	Hot-humid	Pirot-Berson et al. (2024) and Hacke et al. (2024), laboratory

3.1 Potential-induced degradation

PID arises when a high voltage between the cell circuit and the grounded frame drives ionic current through the glass and encapsulant. In p-type crystalline silicon, the dominant form is PID-shunting, in which sodium ions migrate through the silicon nitride antireflection layer and decorate stacking faults that cross the p-n junction, creating shunt paths (Luo et al., 2017). The leakage current follows an Arrhenius dependence on temperature with an activation energy of roughly 0.7 to 0.9 eV at high relative humidity, and leakage at high humidity is several orders of magnitude larger than at low humidity, mainly because the glass surface becomes conductive (Luo et al., 2017). Accelerated testing has quantified the joint temperature and humidity dependence and shown that degradation rates can be modelled as a function of both (Hacke et al., 2015). These laboratory dependences imply that hot-humid Asia carries a high PID hazard, and the field evidence is consistent with this. In the 2018 Indian survey, PID was identified at 7 of 36 sites and was among the most frequent dominant modes at sites with above-median degradation (NCPRE & NISE, 2019). A field study after more than ten years in Singapore attributed a mono-crystalline power loss exceeding 40 percent partly to PID, and found a copper indium selenide module with PID signatures that had lost about 45 percent (Luo et al., 2021); each result rests on two modules per type. Outside Asia, a 1.2 MW plant in Barcelona showed performance-ratio losses of about 27 to 39 percent in PID-affected strings within months of operation, illustrating how quickly PID can act once leakage conditions are present (Badran & Dhimish, 2022). A plausible implication for humid Asia, not yet tested directly, is that early-morning dew rather than average humidity is the operative stressor, so mean climate statistics would underestimate PID exposure.

3.2 Encapsulant discolouration, delamination and moisture-driven corrosion

EVA encapsulant degrades under the combined action of UV, heat and moisture. Photodegradation generates chromophores that cause yellowing or browning, while hydrolysis produces acetic acid that corrodes cell metallisation and solder (de Oliveira et al., 2018). Moisture enters mainly through breathable backsheets and module edges, and the ingress rate depends on temperature, humidity and polymer permeability (Segbefia et al., 2021). Field-aged multicrystalline modules show moisture-induced degradation patterns that track this ingress (Segbefia et al., 2023). The 2018 Indian survey found encapsulant discolouration in all climatic zones but progressing faster in hot zones, showed that visible discolouration was associated with power loss, found delamination most frequently in warm and humid zones although its prevalence was not high, and reported more metal and interconnect corrosion in hot zones (NCPRE & NISE, 2019). The global review by Jordan et al. (2017) reached a compatible conclusion: discolouration was the most common mode overall and, in newer systems, appeared mainly in hotter climates and to a lesser degree. In Singapore, corrosion around cell edges was the likely cause of a multicrystalline power loss of more than 9 percent after ten years (Luo et al., 2021). Backsheets add a further pathway. At a desert outdoor test facility, polyamide and polyethylene terephthalate backsheets embrittled and cracked from the UV-blocking outer layer inwards, and one showed chalking that reacted with cell interconnects (Abdallah et al., 2024). A review of environmental variables links UV, temperature and humidity to distinct pathways in each module component and argues that reliability assessment should be organised around these variables rather than around generic test sequences (Lyu et al., 2020). The reviewed studies therefore indicate that hot-humid and hot-arid sites stress encapsulation through different pathways, so a single encapsulant choice is unlikely to be optimal across Asia.

3.3 Light- and elevated-temperature-induced degradation and UV-induced degradation

Light-induced degradation (LID) from boron-oxygen complexes has long been understood, but light- and elevated-temperature-induced degradation (LeTID) emerged as a distinct problem with passivated emitter and rear contact (PERC) cells. LeTID develops over months to years at elevated operating temperatures and can partially regenerate, which makes it relevant to hot Asian climates where module temperatures are high for much of the year (Yeo et al., 2022). Cell and process mitigation has reduced its prevalence, yet field exposure records for modern PERC in Asia remain short. UV-induced degradation (UVID) is a newer concern for high-efficiency cell architectures, and the evidence is so far from accelerated laboratory testing. After a UV dose of 4.02 MJ per square metre (2,000 hours), heterojunction, interdigitated back contact, PERC and passivated emitter rear totally diffused cells lost on average about 3.6 percent and at most 11.8 percent of power, whereas conventional aluminium back-surface-field cells lost less than 1 percent on average (Sinha et al., 2023). The same study estimated an acceleration factor of about five between unencapsulated cells in the test and encapsulated modules outdoors, and showed that UV-blocking encapsulants reduce transmitted UV by a further factor of about fifty. Mechanistic work has also examined how UVID arises in HJT cells (Yang et al., 2024). This produces a design tension: UV-transparent encapsulants protect against browning but expose cells to UVID, while UV-blocking encapsulants do the opposite. In the high-UV Gulf and Thar deserts, no field data were located that resolve the balance between these two risks.

3.4 Bifacial, TOPCon and heterojunction specific risks

The shift to bifacial glass-glass modules and n-type cells changes rather than removes climatic risk. Glass-glass construction reduces moisture ingress through the rear, but it does not eliminate PID. In an outdoor test in humid subtropical Florida, bifacial PERC modules held at an applied -1500 V bias lost a mean of about 4.5 to 6 percent of front-side power at standard test conditions, mostly

within the first 2.5 weeks, by polarisation-type PID; modules elevated about 2 m above ground, which received about twice the rear albedo irradiance, degraded slightly more slowly but reached a similar level (Hacke et al., 2025). Higher morning leakage on near-ground modules was linked to longer dew persistence, a finding relevant to humid Asian sites. Because the bias was applied deliberately, this is a field-exposed stress test rather than a measurement of operating-fleet degradation. In the laboratory, TOPCon modules show reversible front-side PID-polarisation: about 30 percent power loss under -1000 V at 60 degrees Celsius for 96 hours in the dark, but only a 3 percent mean loss under the same bias with UVA, with activation energies of 0.71 eV for degradation and 0.58 eV for recovery (Hacke et al., 2024). HJT modules fail in damp heat through sodium and moisture effects on their thin layers (Pirot-Berson et al., 2024), and their UVID mechanism has been investigated at cell level (Yang et al., 2024). Figure 1 presents the magnitudes reported for these modes, with accelerated laboratory results in panel (a) and field exposure in panel (b); the two panels are not directly comparable, since a laboratory loss reflects the stress applied rather than a time in service. Because TOPCon now dominates new Asian supply, the scarcity of multi-year field data for it in hot-humid climates is a major evidence gap.

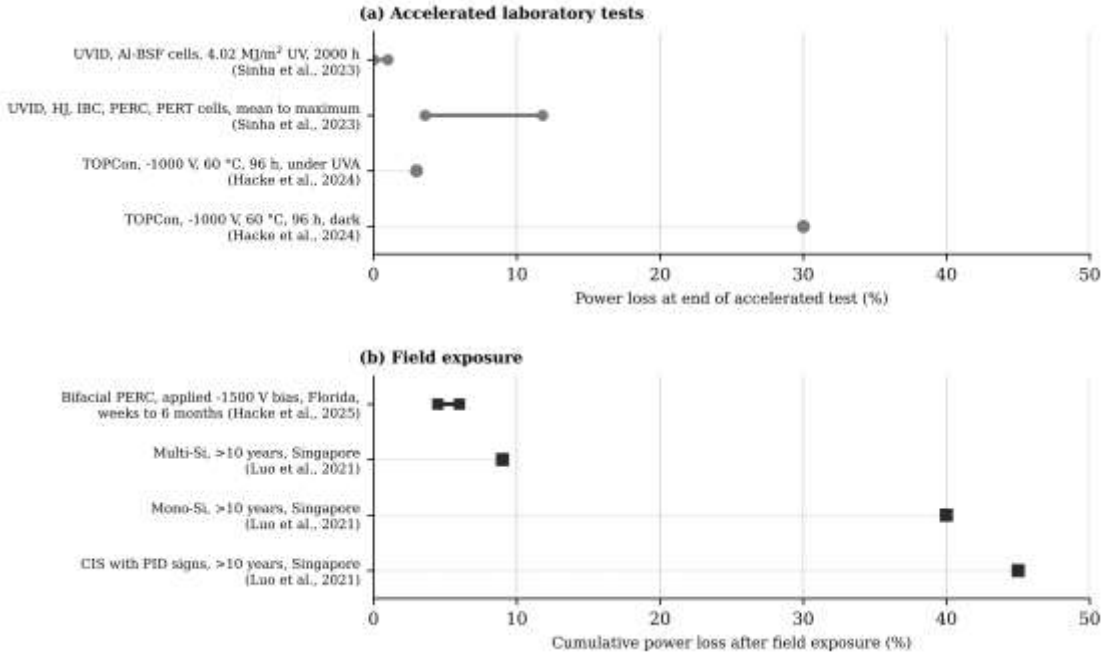


Figure 1. Reported power losses attributed to specific degradation modes. (a) Accelerated laboratory stress tests: loss at the end of the stated test (circles). (b) Field exposure: cumulative loss after the stated period in service (squares); the Florida result is from modules held at an applied bias outdoors. Horizontal bars show mean to maximum or reported spread; single markers show single reported values. The panels measure different quantities and should not be compared directly. Measured data from Sinha et al. (2023), Hacke et al. (2024), Hacke et al. (2025) and Luo et al. (2021).

4. Field degradation rates measured in Asia

Field degradation rates link mechanisms to money, yet they are among the most method-sensitive numbers in PV engineering. The same dataset can yield different rates depending on whether the analyst uses performance ratio, regression on corrected power, or year-on-year methods, and on how irradiance and temperature corrections are made (Daher et al., 2022). Comparisons across studies therefore require attention to method before attention to climate. Global syntheses provide the benchmark: a crystalline silicon median of 0.5 to 0.6 percent per year (Jordan et al., 2016), a fleet median of 0.58 percent per year for recent technologies (Theristis et al., 2023) and a meta-analytic median of 0.94 percent per year (Straub-Mück et al., 2025). Table 3 and Figure 2 set field-measured Asian rates against these benchmarks; all values in this section are field observations, not laboratory results. The subsections define the estimation method, examine South Asia, Southeast Asia and desert sites, and then assess comparability.

4.1 Estimating degradation rates

The most common estimator in the Asian literature regresses a temperature- and irradiance-corrected performance metric against time. Monthly corrected power or performance ratio values are fitted with an ordinary least-squares line:

$$P_c(t) = \beta_0 + \beta_1 t + \varepsilon_t \qquad (1)$$

In Equation (1), $P_c(t)$ is the corrected power in watts (or the dimensionless performance ratio) in month t, β_0 is the intercept representing initial performance in the same units, β_1 is the slope in those units per month, and ε_t is the residual. The annual degradation rate follows as:

$$R_d = \frac{12\,\beta_1}{\beta_0} \times 100 \qquad (2)$$

In Equation (2), R_d is the annual degradation rate in percent per year, with a negative sign denoting loss, and the factor 12 converts the monthly slope to an annual value; the ratio β_1/β_0 has units of per month, so R_d is dimensionally a percentage per year. The estimator is simple but sensitive to seasonality, soiling and outliers. The Djibouti comparator illustrates the problem: the same five-year record produced 1.01 plus or minus 0.38 percent per year from performance ratio regression, 0.085 plus or minus 0.68 percent per year (not statistically meaningful) from PVUSA regression, and 0.74 plus or minus 0.29 percent per year with test conditions redefined from local data (Daher et al., 2022). Reviews of methodology have urged reporting of uncertainty and method alongside every rate (Jordan & Kurtz, 2013; Kumar & Kumar, 2017). Rates from single-time-point flash tests of field-aged modules, as used in national surveys, avoid seasonal confounding but assume a nameplate baseline that may itself be inaccurate (Jordan et al., 2016).

4.2 South Asia

India provides the deepest climate-stratified evidence in Asia (evidence level A). The 2014 All-India survey of more than 1,000 modules found an average rate of 1.33 percent per year for good-quality modules, with hot zones averaging 1.42 percent per year against 1.05 percent per year for non-hot zones, about 35 percent higher (Dubey et al., 2017). In the hot zone, modules without hot cells averaged 1.39 and modules with hot cells 2.02 percent per year. System size mattered at least as much as climate: across all zones, installations above 100 kWp averaged 0.97 percent per year and smaller ones 2.3 percent per year, and large systems showed almost similar rates in hot and non-hot climates, whereas small systems were more climate-sensitive (Dubey et al., 2017). The 2018 survey analysed 1,199 modules (1,094 crystalline silicon) at 36 sites aged from about one to more than 25 years; crystalline silicon degraded at 1.47 percent per year on a linear basis, against an international benchmark cited as about 0.6 to 0.8 percent per year, roof-mounted modules at 1.99 and ground-mounted at 1.33 percent per year, and modules aged one to five years faster (1.85) than older modules (1.14 percent per year) (NCPRE & NISE, 2019). The survey bounded measurement and translation error at 6 percent for measurements above 700 W per square metre, but did not fully quantify nameplate tolerance and initial LID. A twelve-year study at one site in India's composite climate found 1.50 percent per year for multicrystalline silicon, 1.24 for amorphous silicon and 0.14 for HIT modules (Singh et al., 2022). In the reviewed Indian studies, then, the climate gap (0.37 percentage points between zones) was smaller than the size gap (1.33 points) and the mounting gap (0.66 points), so climate is associated with faster degradation but does not explain most of the variation.

4.3 Southeast and East Asia

Evidence from the humid tropics is thinner and more dispersed. At Thailand Science Park, degradation rates ranged from 0.5 to 4.9 percent per year across module types, implying a 10 to 50 percent output loss over 25 years (Limmanee et al., 2016). A four-year follow-up of 73 modules of four technologies found 0.3 to 1.9 percent per year for most modules, while some micromorph thin-film modules failed outright (Limmanee et al., 2017). In Singapore, seven-year monitoring of five crystalline silicon modules, one of each type, found temperature-corrected performance-ratio rates of 0.03 to 0.47 percent per year, within warranty (Luo et al., 2019). A separate study of two modules each of three types after more than ten years found losses of more than 9 percent for multicrystalline silicon, more than 40 percent for mono-crystalline silicon and about 45 percent for one copper indium selenide module, driven by corrosion, discolouration and PID (Luo et al., 2021); expressed as linear equivalents these are roughly 0.9, 4.0 and 4.5 percent per year. The contrast between these two Singapore datasets is large: the same climate produced near-benchmark and severe outcomes. It is consistent with bill of materials and module vintage being major variables, but neither design can separate them from manufacturer and installation effects. Malaysian field work dates mainly from a three-day technology comparison (Amin et al., 2009), so long-term Malaysian rates were not located in the peer-reviewed literature. For Vietnam, Indonesia, the Philippines and Bangladesh, peer-reviewed multi-year degradation rates were not located either, which means the fastest-growing tropical markets are planning with rates measured elsewhere. In the reviewed tropical studies, the most defensible reading is that the humid tropics impose a higher degradation hazard, that well-specified modules can perform close to the global benchmark, and that poorly specified ones can fail early and severely (Limmanee et al., 2016, 2017).

4.4 Desert sites in and near Asia

Peer-reviewed long-term degradation rates from hot-arid Asian sites are scarce in the reviewed set. In the Gobi Desert of Mongolia, a cold and dry rather than hot site, two crystalline modules monitored from 2002 to 2012 degraded at 1.28 and 0.86 percent per year, with performance ratios of 0.85 and 0.80 (Bayandelger et al., 2018). The Djibouti comparator, a desert maritime site resembling coastal Gulf locations, reported 0.74 to 1.01 percent per year for a 302.4 kWp plant depending on method (Daher et al., 2022). A seven-year tracking test in a desert climate found that measurement reproducibility and nameplate tolerance materially change whether modules meet a 30-year warranty, and that 0.4 to 0.6 percent per year was compatible with such a warranty under positive-only tolerance (Huang et al., 2023); this is a warranty scenario rather than a measured fleet rate. Gulf evidence is dominated by soiling studies rather than by clean degradation measurements, because uncleaned arrays in Qatar lost half their output within eight months, which overwhelms the slower degradation signal (Touati et al., 2017). Backsheet studies at a desert test facility show the materials pathway through which degradation proceeds even where electrical rates appear modest (Abdallah et al., 2024). Taken together, Table 3 and Figure 2 indicate that the few desert records reviewed report 0.74 to 1.28 percent per year, but none is from a hot-arid Asian site with a multi-site design, so desert-Asia rates remain weakly evidenced.

Table 3. Field-measured degradation rates at Asian and comparator sites, with sample, technology generation, estimation method, uncertainty where reported, and evidence level (Table 1).

Location and climate	Technology and sample	Period and method	Rate (%/year) and uncertainty	Source (level)
India, hot zones	c-Si, installed before 2014, subset of more than 1,000 modules	Single-time flash test against nameplate	1.42 (not reported)	Dubey et al. (2017) (A)
India, non-hot zones	c-Si, same survey	As above	1.05 (not reported)	Dubey et al. (2017) (A)
India, 36 sites	c-Si, 1,094 modules aged 1 to 25+ years	Linear, flash test against nameplate	1.47 (measurement error up to 6%)	NCPRE & NISE (2019) (A)
India, composite	mc-Si, a-Si, HIT, one site	12 years, end-point I-V	1.50, 1.24, 0.14 (not reported)	Singh et al. (2022) (B)
Thailand, tropical	Four technologies, 73 modules	4 years, periodic I-V	0.3 to 1.9 (array spread)	Limmanee et al. (2017) (B)
Thailand, tropical	Several module types	Multi-year, periodic I-V	0.5 to 4.9 (range)	Limmanee et al. (2016) (B)
Singapore, tropical	c-Si, 5 modules, one per type	7 years, temperature-corrected PR	0.03 to 0.47 (range)	Luo et al. (2019) (B)
Mongolia, Gobi (cold-arid)	c-Si, 2 modules	10 years, PR and yield	0.86 to 1.28 (range)	Bayandelger et al. (2018) (B)
Djibouti, desert maritime	302.4 kWp plant	5 years, PR and PVUSA regression	0.74 ± 0.29 to 1.01 ± 0.38	Daher et al. (2022) (B)
Global benchmark	c-Si, more than 11,000 rates	Compilation	0.5 to 0.6 (median)	Jordan et al. (2016) (A)

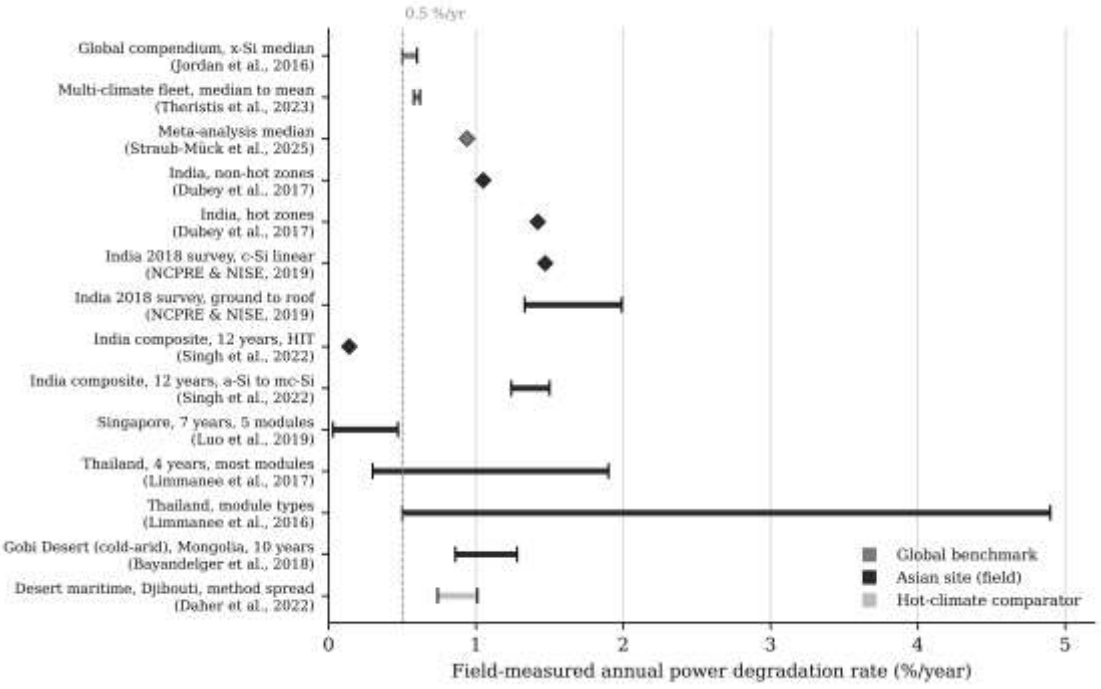


Figure 2. Field-measured annual degradation rates at Asian sites compared with global benchmarks and a hot-climate comparator; no accelerated laboratory results are included. Bars show reported ranges; diamonds show single values. The dashed line marks 0.5 percent per year. Sample sizes, methods and uncertainties differ between studies (Table 3), so the bars are not equally precise. Measured data from Jordan et al. (2016), Theristis et al. (2023), Straub-Mück et al. (2025), Dubey et al. (2017), NCPRE and NISE (2019), Singh et al. (2022), Luo et al. (2019), Limmanee et al. (2016, 2017), Bayandelger et al. (2018) and Daher et al. (2022).

4.5 Comparability of reported rates

The rates in Table 3 are not equally comparable, for four reasons. First, sample size varies by three orders of magnitude, from two modules in the Gobi study to more than 1,000 in each Indian survey, and single-site studies with one or two modules per type cannot separate climate from manufacturer effects (Bayandelger et al., 2018; Luo et al., 2019). Second, technology generation differs: the Indian surveys examined modules installed up to about 2017, predominantly multicrystalline (874 of 1,094 crystalline modules in 2018), and the ten-year Singapore study examined modules with more than a decade in service by 2021, whereas the fleet benchmark of Theristis et al. (2023) covers recent technologies, and no field rate for TOPCon in hot Asian climates was located. Third, estimation method changes the result: single-time flash tests against nameplate absorb nameplate tolerance and initial LID into the rate, while regression on performance ratio absorbs soiling and seasonal effects (Jordan et al., 2016; Daher et al., 2022). The 2018 Indian survey shows the effect of the baseline assumption, reporting 1.47 percent per year after discounting initial LID but 1.93 percent per year without (NCPRE & NISE, 2019). Fourth, uncertainty is reported in only a minority of the reviewed Asian studies, and where reported it can be as large as the rate itself (Daher et al., 2022). For these reasons this review compares rates only within like designs and treats the Indian surveys as the strongest Asian evidence. On that basis, the measured averages are about 2.2 to 2.9 times the global median of 0.5 to 0.6 percent per year, while the dispersed tropical evidence supports no single multiplier.

5. Soiling losses and cleaning strategies

Soiling is the accumulation of dust, pollen, bird droppings, biological growth and anthropogenic particulates on the module surface. It is reversible in principle, which is why it is often treated as an operations issue separate from degradation. That separation is analytically convenient but physically incomplete for hot Asian climates. Even with optimised cleaning, soiling has been estimated to reduce global solar production by at least 3 to 4 percent, with annual revenue losses of at least 3 to 5 billion euro, and this share was projected to rise to 4 to 7 percent as deployment concentrates in high-soiling regions (Ilse et al., 2019). Many of those regions are in Asia and the Middle East. Soiling also interacts with degradation: dew-driven cementation alters the glass surface, and cleaning itself can abrade glass and coatings (Ilse et al., 2018b; Bomber et al., 2024). The subsections below treat measurement, measured losses and mitigation.

5.1 Soiling physics and measurement

Soiling losses depend on deposition rate, particle size and composition, adhesion and removal by wind and rain. Fundamental work distinguishes the deposition, adhesion and removal stages and shows that adhesion forces increase sharply when moisture is present (Ilse et al., 2018a). In Qatar, frequent dew formation drives cementation of dust by palygorskite clay crystals that form on the glass, and heating samples to prevent dew inhibited cementation and substantially reduced accumulation (Ilse et al., 2018b). A global review concluded that soiling accounts for most of the combined power reduction from soiling and air pollution in most regions, the exception being highly polluted areas where atmospheric attenuation is the larger factor (Song et al., 2021). Soiling also changes the electrical behaviour of a module in ways that depend on how uniformly dust is distributed. Uniform deposits act as soft shading, reducing current without changing voltage, whereas concentrated deposits such as bird droppings or soiling bands along the lower frame edge act as hard shading on individual cells, activating bypass diodes and creating hot spots (Maghami et al., 2016). The standard metric is the soiling ratio:

$$SR = \frac{I_{sc,s}/G_s}{I_{sc,c}/G_c} \qquad (3)$$

In Equation (3), SR is the dimensionless soiling ratio, $I_{sc,s}$ and $I_{sc,c}$ are the short-circuit currents in amperes of a naturally soiled reference device and of a regularly cleaned device, and G_s and G_c are the corresponding plane-of-array irradiances in watts per square metre. The soiling loss is then $1 - SR$. Short-circuit current is preferred to maximum power because it is nearly linear in transmitted irradiance and less sensitive to temperature. Where dedicated soiling stations are absent, losses must be inferred from system yield, and modelling reviews show that predictive soiling models remain site-calibrated rather than transferable (Dehghan et al., 2022; Conceição et al., 2022).

5.2 Measured soiling losses at Asian sites

Reported losses span almost an order of magnitude because exposure periods, tilt and metrics differ, as Table 4 and Figure 3 show; all are field or outdoor measurements except where stated. In the United Arab Emirates, indoor tests found a 1.7 percent drop in normalised power per gram of dust per square metre, five months of outdoor exposure increased soiling loss by 12.7 percent, and horizontal modules were affected far more than tilted ones (Hachicha et al., 2019). In Sharjah, glass transmittance fell by 30 percent after 15 weeks, with silica and calcite dominant (Dhaouadi et al., 2021). In Qatar, unclean modules lost 43 percent of output after six months (Zeedan et al., 2021) and 50 percent over an eight-month dusty period (Touati et al., 2017), while one month without cleaning reduced the performance ratio by up to about 15 percent in a comparison of heterojunction and conventional modules (Abdallah et al., 2016). In Lahore, Pakistan, a 100-day experiment produced energy losses of 26.2 percent for a horizontal panel and 13.5 percent for a vertical one, relative to a clean panel (Ullah et al., 2019). In East China, an average weekly dust density of 0.644 g per square metre was estimated to reduce output by 7.4 percent in a week (Chen et al., 2020). Humid urban settings show a different pattern: over 108 days in a high-density city, rainwater residue caused optical losses within 2 percent, whereas a tiny residue of bird droppings caused a 2.5 percent optical and a 15.5 percent output loss (Li et al., 2024). Across the reviewed sites, soiling in the Gulf exceeded a year of degradation within weeks to months, while in the humid urban study it was smaller but more heterogeneous.

Table 4. Soiling losses and cleaning-related findings reported for Asian and Middle Eastern sites (all relative to a clean reference unless stated).

Site	Exposure	Reported loss	Metric	Source
Doha, Qatar	6 months, uncleaned	43%	Power output	Zeedan et al. (2021)
Qatar	8 months, dusty	50%	Power output	Touati et al. (2017)
UAE	5 months, outdoor	12.7% increase	Soiling loss	Hachicha et al. (2019)
Sharjah, UAE	15 weeks	30%	Glass transmittance	Dhaouadi et al. (2021)
Lahore, Pakistan	100 days, horizontal	26.2%	Energy yield	Ullah et al. (2019)
East China	1 week	7.4% (estimated)	Power output	Chen et al. (2020)
Asia and MENA, optimal cleaning	Every 5 to 6 days	2.5% median	Revenue	Mithhu et al. (2021)

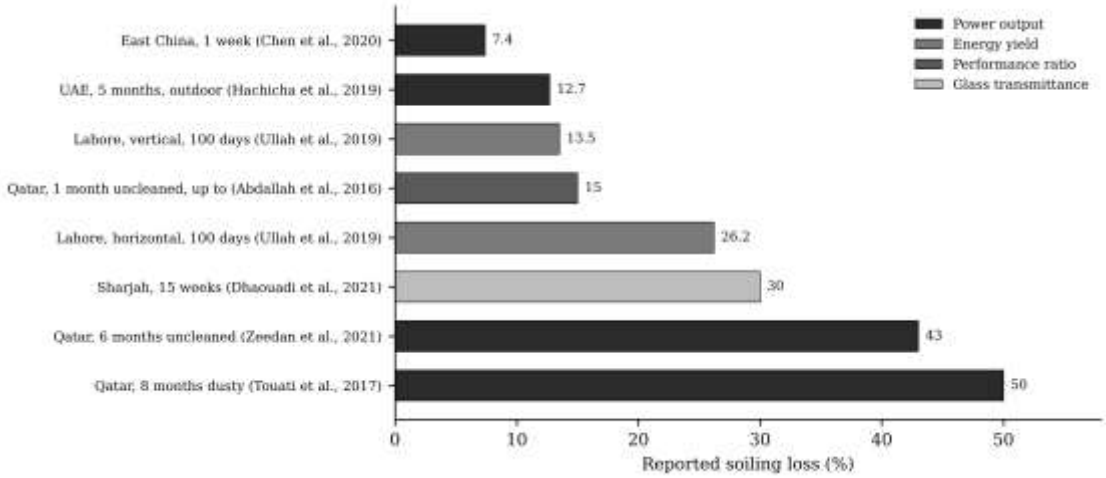


Figure 3. Field-measured soiling losses at Asian and Middle Eastern sites, shaded by the metric used. Losses are relative to a clean reference over the stated exposure; the metrics differ and are not interchangeable. Measured data from Chen et al. (2020), Hachicha et al. (2019), Ullah et al. (2019), Abdallah et al. (2016), Dhaouadi et al. (2021), Zeedan et al. (2021) and Touati et al. (2017).

5.3 Water-scarce cleaning and anti-soiling coatings

Cleaning frequency is an economic optimisation between energy recovered and the cost of cleaning. A global analysis found that median revenue loss from soiling in Asia and the Middle East and North Africa remains 2.5 percent even with optimal cleaning every 5 to 6 days, compared with 1.5 percent at a 12-day interval in the United States, and that optimally cleaned farms lose 2 to 5 percent of revenue once regional cleaning costs are included (Mithhu et al., 2021). In Jordan, model-based analysis estimated that dust reduced efficiency by about 0.61 to 0.77 percent per day and identified an optimal cleaning interval of 12 to 15 days (Hammad et al., 2018). Dynamic, season-dependent schedules outperform fixed intervals (Kaiss & Hassan, 2024; Astete et al., 2024). Water is the binding constraint in desert Asia. In Las Vegas, cleaning with groundwater and treated wastewater recovered less efficiency than distilled water, and dissolved minerals appeared to reduce performance (Boeing et al., 2022), which warns against assuming that any available water source is suitable. Anti-soiling coatings offer an alternative: in laboratory tests, three coatings reduced dust deposition density on glass to 36 to 51 percent of that on bare glass (Pan et al., 2019). Durability is the limiting factor. Reviews identify durability as the central barrier to superhydrophobic polymers (Cherupurakal et al., 2021), and a five-year field study of coated glass in Dubai, Kuwait City and Mumbai, alongside two United States sites, found cleaning methods easier to distinguish than coatings and quantified abrasion from dry brushing (Bomber et al., 2024). Reviews of cleaning methods conclude that no single technique is optimal across dust types and climates (He et al., 2023; Costa et al., 2018), and the dew-driven cementation documented in Qatar suggests that dry methods lose effectiveness where water is scarcest. Rain provides partial natural cleaning in the monsoon belt, and East Chinese measurements were designed to separate dust accumulation from rainfall effects (Chen et al., 2020); together with the seasonal optimisation literature, this implies seasonal rather than fixed cleaning schedules for South Asian sites with long dry seasons (Mithhu et al., 2021).

6. Thermal effects and climate-specific qualification testing

Temperature affects PV modules twice: instantaneously, by reducing conversion efficiency, and cumulatively, by accelerating the chemical and mechanical degradation reviewed above. The instantaneous effect is large in hot Asian climates. A Thai study found that modules with a power temperature coefficient below -0.31 percent per degree Celsius had an energy-yield advantage under tropical conditions (Limmanee et al., 2016), and a one-year comparison in a hot Moroccan desert found cadmium telluride less affected by temperature than polycrystalline silicon (Mehdi et al., 2023). The cumulative effect is what qualification tests try to screen. This section sets out the thermal models used to correct field data and estimate operating temperature, then evaluates whether the current IEC qualification standards and emerging climate-specific sequences represent Asian stresses (Makhija & Bohra, 2023).

6.1 Module temperature and temperature-corrected performance

Two models dominate practice. The nominal operating cell temperature (NOCT) approach estimates cell temperature as:

$$T_c = T_a + \frac{NOCT - 20}{800} G \qquad (4)$$

In Equation (4), T_c is the cell temperature in degrees Celsius, T_a is the ambient temperature in degrees Celsius, $NOCT$ is the nominal operating cell temperature in degrees Celsius specified by the manufacturer, 20 and 800 are the reference ambient temperature (degrees Celsius) and irradiance (watts per square metre) at which NOCT is defined, and G is the plane-of-array irradiance in watts per square metre. The NOCT model ignores wind, which matters in open desert sites. The Faiman model incorporates it:

$$T_m = T_a + \frac{G}{U_0 + U_1 v} \qquad (5)$$

In Equation (5), T_m is the module temperature in degrees Celsius, U_0 is the constant heat loss coefficient in watts per square metre per degree Celsius, U_1 is the wind-dependent coefficient in watts per square metre per degree Celsius per metre per second, and v is the wind speed in metres per second. Faiman (2008) fitted these coefficients to outdoor data for silicon modules in the Negev desert. With a module temperature estimate, measured power can be translated to standard test conditions:

$$P_{25} = \frac{P_m}{(G/G_{STC})[1 + \gamma(T_m - 25)]} \qquad (6)$$

In Equation (6), P_{25} is the power in watts corrected to 25 degrees Celsius and standard irradiance, P_m is the measured power in watts, G_{STC} is 1000 watts per square metre, and γ is the power temperature coefficient per degree Celsius. Most of γ reflects the recombination-driven fall in open-circuit voltage with temperature (Atta et al., 2024). Reviews of efficiency and power correlations show that γ and the thermal model choice can shift corrected values by several percent (Skoplaki & Palyvos, 2009), so in hot climates the correction error can be comparable in size to several years of degradation. The performance ratio is defined as $PR = (E_{AC}/P_0)/(H/G_{STC})$, where E_{AC} is AC energy delivered in kilowatt-hours, P_0 is nameplate power in kilowatts and H is plane-of-array insolation in kilowatt-hours per square metre; it bundles thermal, soiling and degradation losses unless each is corrected separately.

Thermal behaviour in the field departs from these models in ways that matter for Asian sites. Rooftop arrays in dense Indian and Southeast Asian cities are often mounted close to the roof with little ventilation. In the 2018 Indian survey, roof-mounted modules degraded at 1.99 percent per year against 1.33 percent per year for ground-mounted ones, a difference consistent with a thermal contribution, although installation quality is a confounding factor and the survey design cannot establish causation (NCPRE & NISE, 2019). Analysis for IEC TS 63126 compliance shows that poor airflow in close-roof systems in hot climates can push the 98th percentile module temperature above 70 degrees Celsius, and proposes a minimum standoff height to avoid this (Kempe et al., 2024). In the humid tropics, low wind reduces convective cooling, so coefficients fitted at windy desert sites may overestimate heat loss. In hot deserts, the large diurnal swing imposes a thermal cycle every day, which can fatigue interconnects and solder bonds (Mehdi et al., 2023). Thermal models therefore need local calibration before they are used to correct degradation estimates (Skoplaki & Palyvos, 2009).

6.2 IEC qualification standards and their climatic limits

IEC 61215 is a design qualification standard, not a lifetime test; its current edition (Ed. 2.0) was published in February 2021 as IEC 61215-1 (test requirements) and IEC 61215-2 (test procedures), cancelling and replacing the 2016 first edition (IEC, 2021). Table 5 lists the requirements. The damp heat test (MQT 13) exposes modules for 1,000 hours at 85 degrees Celsius and 85 percent relative humidity; thermal cycling (MQT 11) runs 200 cycles between -40 and 85 degrees Celsius; humidity freeze (MQT 12) runs 10 cycles from 85 degrees Celsius and 85 percent relative humidity to -40 degrees Celsius; and UV preconditioning (MQT 10) applies at least 15 kWh per square metre between 280 and 400 nm at a module temperature of about 60 degrees Celsius (IEC, 2021); the damp heat and thermal cycling conditions are also reported in recent peer-reviewed testing (Nam et al., 2025). The 2021 edition added a PID test (MQT 21), cyclic mechanical loading, and methods for bifacial and flexible modules (IEC, 2021). The PID test applies the method of IEC TS 62804-1, whose first edition stressed modules at maximum system voltage, 60 degrees Celsius and 85 percent relative humidity for 96 hours (Yilmaz et al., 2022); the second edition (Ed. 2.0, June 2025) specifies dark tests for PID-shunting, UV-illuminated tests for polarisation-type PID and a UV recovery test, and states that the tests measure susceptibility rather than predict field performance in a given climate (IEC, 2025b). Safety qualification under IEC 61730-1:2023 (Ed. 3.0) applies to modules whose 98th percentile operating temperature (T98) is 70 degrees Celsius or less and refers hotter applications to IEC TS 63126 (IEC, 2023), whose second edition of October 2025 replaces the 2020 first edition and defines Level 1 for T98 up to 80 degrees Celsius and Level 2 up to 90 degrees Celsius (IEC, 2025a).

Several features limit the relevance of this framework to Asian climates. First, the UV preconditioning step was designed to precondition modules, not to test UV durability, and accelerated UVID tests show that architectures able to pass qualification can still lose several percent under extended UV exposure (Sinha et al., 2023). Second, the PID test uses dark, damp-heat conditions and, by the specification's own statement, does not represent a particular climate, so dew-driven leakage at humid sites may be underrepresented (IEC, 2025b; Hacke et al., 2015). Third, the standard applies one or two stresses at a time, whereas field degradation results from simultaneous stresses; combined-accelerated stress testing reproduced backsheet cracking and other field failures that standard sequences missed (Owen-Bellini et al., 2021), and combined light and damp heat cycling produced 3.51 percent power loss against 0.87 percent after 1,000 hours of damp heat and 1.32 percent after 200 thermal cycles for the same module type (Nam et al., 2025). Fourth, abrasion from cleaning and sandstorms is absent. The Indian survey's finding that crystalline silicon modules degraded at about twice the international benchmark (NCPRE & NISE, 2019) is consistent with the view that qualification alone does not ensure benchmark performance in hot climates. Qualification also addresses design rather than production consistency: modules of nominally similar type showed widely differing rates in the Indian and Singapore datasets (Dubey et al., 2017; Luo et al., 2019, 2021), so factory audits, batch testing and incoming electroluminescence inspection matter alongside the choice of test sequence.

Table 5. Qualification stresses in the current IEC editions (IEC 61215-2:2021 Ed. 2.0; IEC 61730-1:2023 Ed. 3.0; IEC TS 62804-1:2025 Ed. 2.0; IEC TS 63126:2025 Ed. 2.0) compared with extensions indicated for Asian hot-humid and hot-arid climates (requirements from IEC, 2021, 2023, 2025a, 2025b; Nam et al., 2025; Yilmaz et al., 2022).

Stress	Current requirement	Hot-humid extension	Hot-arid extension
Damp heat (MQT 13)	1,000 h, 85 C, 85% RH	Longer duration with system bias	Combined with UV
PID (MQT 21)	Added in IEC 61215-2:2021; method of IEC TS 62804-1 (Ed. 2.0, 2025, includes UV-illuminated tests)	Dew and wet-surface conditions, both polarities	Night-time dew on soiled glass
UV preconditioning (MQT 10)	At least 15 kWh/m2, 280 to 400 nm, about 60 C	Moderate dose after damp heat	Extended dose for UVID and browning
Thermal cycling (MQT 11)	200 cycles, -40 to 85 C (sequence D)	Standard	Higher-temperature cycling where T98 exceeds 70 C
Humidity freeze (MQT 12)	10 cycles, 85 C and 85% RH to -40 C	Standard	Standard
High temperature	IEC 61730-1:2023 limit T98 of 70 C; IEC TS 63126:2025 (Ed. 2.0) Level 1 up to 80 C, Level 2 up to 90 C	Close-roof arrays	Ground and rooftop arrays
Abrasion and soiling	Not included	Biological and bird-dropping residue	Sand abrasion, cleaning wear, cementation

6.3 Toward climate-specific stress testing

Three developments point towards climate-specific qualification. The first is climate-specific accelerated ageing, which sets test durations and stress levels from the stress profiles of target climates; Eder et al. (2019) designed such sequences for different climate zones and evaluated the electrical, physical and chemical changes they induced. The second is the desert label initiative, which combines high UV dosage with damp heat, salt mist or aggressive thermal cycling for harsh desert conditions and checks indoor results against outdoor monitoring of sister mini-modules in the Atacama Desert (Lelièvre et al., 2022). The third is combined testing for new technologies: TOPCon PID-polarisation testing that combines bias, temperature and UV (Hacke et al., 2024), UVID protocols that expose architecture-specific weaknesses (Sinha et al., 2023), and combined-accelerated stress testing with tropical and multi-season phases (Owen-Bellini et al., 2021). Table 5 lists the extensions these studies imply for each Asian climate family. The desert label targets the Atacama, whose dust and humidity differ from the Gulf's dew-driven clay cementation (Ilse et al., 2018b). An Asian hot-humid label was not found in the peer-reviewed literature, although the field evidence reviewed points to PID and moisture corrosion as dominant modes there (Luo et al., 2021).

7. Economic consequences

Degradation and soiling affect project economics through the energy denominator of the levelised cost. The effect compounds because degradation reduces output in every year after it occurs and soiling losses recur unless they are paid for through cleaning. A climate-resolved LCOE can be written as:

$$LCOE = \frac{C_0 + \sum_{t=1}^{N} \frac{O_t + K_t}{(1+r)^t}}{\sum_{t=1}^{N} \frac{E_1 (1 - R_d)^{t-1} \overline{SR_t}}{(1+r)^t}} \qquad (7)$$

In Equation (7), $LCOE$ is in currency per kilowatt-hour, C_0 is the initial capital cost per kilowatt of capacity, O_t is the operating and maintenance cost in year t excluding cleaning, K_t is the cleaning cost in year t (both per kilowatt per year), r is the real discount rate, N is the project life in years, E_1 is the first-year energy yield of a clean array in kilowatt-hours per kilowatt, R_d is the annual degradation rate expressed as a fraction, and $\overline{SR_t}$ is the mean soiling ratio in year t achieved by the cleaning policy. The exponent $t - 1$ leaves year-one output undegraded. The equation makes explicit that cleaning cost and soiling ratio trade off, and that a higher degradation rate erodes the energy that justifies the capital outlay. In Thailand, measured rates translated into an LCOE of 4.1 to 14 baht per kWh, and PV electricity was found comparable to the retail price without further cost reductions only if degradation stayed at about 0.2 percent per year or lower (Limmanee et al., 2017); a 25-year output loss of 10 to 50 percent at the observed Thai rates could raise LCOE by up to a factor of two (Limmanee et al., 2016). In Qatar, an estimated 10 percent power decrease after six months without cleaning at utility scale would cost about 11,000 Qatari riyals per hour (Zeedan et al., 2021).

A worked sensitivity based on Equation (7) clarifies the magnitudes; Table 6 reports it. The assumptions are a 25-year life, a 7 percent real discount rate, capital cost of 650 US dollars per kW, operation and maintenance of 10 US dollars per kW per year (15.2 percent of discounted lifetime cost), a clean first-year yield of 1,600 kWh per kW and no change in costs between cases. Raising the degradation rate from 0.5 to 1.5 percent per year reduces cumulative undiscounted energy by 10.95 percent and discounted energy by 7.94 percent. Lowering the mean soiling ratio from 0.98 to 0.95, within the range implied by the Gulf and Pakistani measurements (Ullah et al., 2019; Hachicha et al., 2019), removes a further 3.06 percent of energy every year. Together these raise LCOE by 12.06 percent. Because costs are unchanged, the percentage increase depends only on the discount rate and life: it ranged from 10.79 percent (10 percent, 25 years) to 14.48 percent (5 percent, 30 years). Operations and maintenance reviews argue that cleaning, inspection and replacement should be optimised jointly against such losses rather than budgeted as fixed overheads (Peinado Gonzalo et al., 2020; Abdulla et al., 2024).

Table 6. Recomputed LCOE sensitivity to degradation and soiling assumptions (Equation (7); N = 25 years, r = 7 percent, costs held constant).

Case	Degradation (%/year)	Mean soiling ratio	Discounted energy change	LCOE change
Base	0.5	0.98	Reference	Reference (4.38 US cents/kWh)
Higher degradation	1.5	0.98	-7.94%	+8.63%
Higher degradation and soiling	1.5	0.95	-10.76%	+12.06%

8. The Climate-Resolved Reliability and Soiling Assessment (CRRSA) framework

The preceding sections reveal a structural problem. Degradation, soiling and thermal losses are studied by different communities, measured with different metrics and fed into financial models through separate, usually generic, assumptions. Yet they interact: cementation depends on the same dew that is associated with wet-surface leakage, cleaning abrades coatings, and module temperature controls both instantaneous output and the rate of chemical ageing (Ilse et al., 2018b; Bomber et al., 2024; Luo et al., 2017). Operations and maintenance reviews have called for strategies that combine reliability assessment with economic and technical considerations (Abdulla et al., 2024; Peinado Gonzalo et al., 2020). The CRRSA framework is proposed to meet that call for hot Asian climates. Its architecture is shown in Figure 4 and its components are specified in Table 7. Methodologically, it follows the sequence of classical reliability engineering for complex systems, in which failure modes are identified, linked to the stresses that activate them and ranked by consequence before any lifetime or cost estimate is attempted (Gideon et al., 2019).

8.1 Architecture of the framework

CRRSA has four layers linked by a feedback loop. Layer 1, climate stress characterisation, replaces the binary hot and non-hot classification used in many studies with a site stress vector: module temperature distribution (including the 98th percentile used by IEC TS 63126), time of wetness and dew frequency, UV dose, thermal cycle amplitude, dust flux and composition, and wind. The Indian surveys show that climate zone explains part but not all of the variance in degradation (Dubey et al., 2017), and the Qatar evidence shows that dew governs cementation (Ilse et al., 2018b), so a vector is needed rather than a label. Layer 2 comprises three loss channels. Layer 2a estimates the expected degradation rate from the bill of materials and the stress vector, screening for PID, UVID, LeTID and damp heat susceptibility. Layer 2b estimates the soiling trajectory $SR(t)$ from dust flux, composition, dew and coating durability. Layer 2c estimates thermal derating from the Faiman or NOCT model, the temperature coefficient, mounting and bifacial rear gain. The double-headed arrows in Figure 4 represent hypothesised interactions, such as wet, soiled glass altering leakage pathways relevant to PID; these are not yet parameterised. Layer 3 translates the stress vector into a climate-weighted qualification sequence built on IEC 61215 with the extensions in Table 5 (Lelièvre et al., 2022; Eder et al., 2019). Layer 4 combines the outputs in Equation (7) to choose module technology, cleaning interval and warranty terms. Field monitoring feeds back to update the stress vector and loss-channel models.

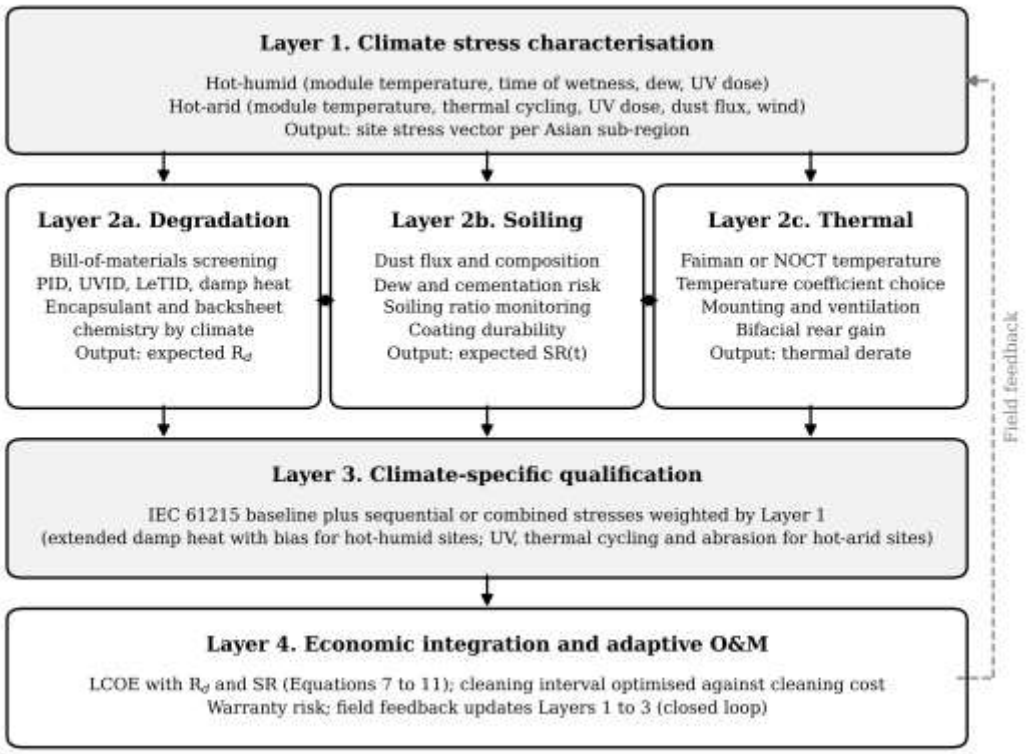


Figure 4. Architecture of the proposed Climate-Resolved Reliability and Soiling Assessment (CRRSA) framework, showing climate stress characterisation, three loss channels, climate-weighted qualification and economic integration with field feedback. Conceptual schematic; no data are plotted.

8.2 Operationalising the framework

Table 7 sets out the inputs, methods and outputs of each layer. Three design choices distinguish CRRSA from existing approaches. First, it treats soiling as a reliability input rather than only an operations cost, because the Gulf evidence shows that soiling losses dominate the energy balance at uncleaned sites (Touati et al., 2017; Zeedan et al., 2021). Second, it requires degradation rates to be reported with method, sample size and uncertainty, following the evidence that method choice alone changed one plant's rate from 0.085 to 1.01 percent per year (Daher et al., 2022). Third, it evaluates cleaning policy jointly with water quality and coating durability, since mineral-rich water and abrasive cleaning can negate gains (Boeing et al., 2022; Bomber et al., 2024). A developer evaluating a TOPCon project in coastal Tamil Nadu would populate Layer 1 with high time of wetness and salt exposure, flag front-side PID-polarisation in Layer 2a (Hacke et al., 2024), specify extended biased damp heat with salt in Layer 3, and test LCOE sensitivity to degradation of 1.0 to 1.9 percent per year in Layer 4, the span of the Indian and Thai field averages, rather than to a datasheet value.

Three limitations apply. The stress vector requires site data on dew frequency and dust composition that few Asian projects collect. The coupling terms between loss channels are documented qualitatively but not yet parameterised (Ilse et al., 2018b; Luo et al., 2017). Climate-weighted qualification adds test cost and duration, which price-competitive procurement may resist unless lenders and insurers reward it (Jordan et al., 2022).

Table 7. Components of the CRRSA framework.

Layer	Inputs	Methods	Outputs
1. Climate stress	Weather, dew, UV, dust flux, wind	Stress vector construction	Site stress profile, T98
2a. Degradation	Bill of materials, stress profile	Mechanism screening, Equations (1) and (2)	Expected degradation rate
2b. Soiling	Dust composition, dew, coating	Equation (3), deposition models	Soiling trajectory
2c. Thermal	Temperature coefficient, mounting	Equations (4) to (6)	Thermal derate
3. Qualification	Stress profile, technology	IEC 61215 plus climate extensions	Pass, fail, risk flags
4. Economics and O&M	Outputs of Layers 2 and 3, costs	Equations (7) to (11), cleaning optimisation	LCOE, cleaning interval, warranty terms

8.3 Illustrative numerical application

To show how CRRSA turns review evidence into decisions, the framework was applied to two illustrative sites, one hot-humid and one hot-arid. The example is illustrative: weather and costs are stated assumptions, other parameters come from the reviewed studies where possible, and the results are not a validation. The three loss channels are combined multiplicatively, which treats them as independent. This simplification suits an illustration because each channel has a separate, documented parameter source, and the reviewed literature quantifies none of the cross-channel couplings in a form that could enter a yield model. The direction and magnitude of the omitted interactions are unknown. Some couplings would increase loss: non-uniform soiling and bird droppings cause hard shading, bypass-diode activation and hot spots that can accelerate local degradation (Maghami et al., 2016; Li et al., 2024), PID leakage and encapsulant ageing are thermally activated and humidity dependent (Luo et al., 2017; Hacke et al., 2015; Segbefia et al., 2021), and dew both cements dust and wets the glass surface that carries PID leakage (Ilse et al., 2018b; Hacke et al., 2025). Others could reduce it: by lowering the irradiance reaching the cells, soiling also lowers module temperature in Equation (5) and hence thermal loss (Faiman, 2008; Mekhilef et al., 2012). The results are therefore neither upper nor lower bounds on combined loss. Annual energy per kilowatt of capacity is:

$$E_t = E_1(1 - R_d)^{t-1}\,\overline{SR} \qquad (8)$$

In Equation (8), E_t is the energy delivered in year t in kilowatt-hours per kilowatt, and E_1, R_d and $\overline{SR}$ are as defined for Equation (7), with the soiling ratio held constant across years. In the base case, soiling is assumed to accumulate linearly at a daily rate s and to be fully removed every τ days, so that:

$$\overline{SR} = 1 - \frac{s\,\tau}{2} \qquad (9)$$

In Equation (9), s is the fractional soiling loss per day and τ is the cleaning interval in days, so $s\tau$ is dimensionless. The clean first-year yield is obtained from the thermal channel using an hourly synthetic year:

$$E_1 = \frac{P_0}{G_{STC}}\,\eta_{BOS} \sum_{h=1}^{8760} G_h\left[1 + \gamma\left(T_{m,h} - 25\right)\right]\Delta t \qquad (10)$$

In Equation (10), P_0 is the nameplate power of 1 kW, G_{STC} is 1,000 watts per square metre, η_{BOS} is the dimensionless balance-of-system and other non-thermal loss factor, G_h is plane-of-array irradiance in hour h in watts per square metre, $T_{m,h}$ is the module temperature in hour h from Equation (5) in degrees Celsius, γ is the power temperature coefficient per degree Celsius, and Δt is one hour, so E_1 is in kilowatt-hours per kilowatt. The annual cleaning cost is:

$$K = c_k \, n_c \qquad (11)$$

In Equation (11), K is the annual cleaning cost in US dollars per kilowatt per year, c_k is the cost per cleaning event in US dollars per kilowatt, and n_c is the number of cleaning events per year, equal to $365/\tau$ in the base case. The hourly year is deterministic and synthetic: irradiance follows a half-sine between 06:00 and 18:00 scaled by a seasonal amplitude and a monthly clearness factor (lower during the monsoon at the hot-humid site), ambient temperature follows a daily sinusoid with a 15:00 maximum around a seasonal mean, and wind speed has a daily cycle peaking in mid-afternoon. These profiles are assumptions chosen to be plausible for coastal South or Southeast Asia and for the Gulf or Thar, not measured weather. Three decision rules are applied. Rule 1 computes the 98th percentile of module temperature over operating hours (irradiance above zero), the quantity used by IEC 61730-1 and IEC TS 63126, and assigns no extension (70 degrees Celsius or less), Level 1 (up to 80 degrees Celsius) or Level 2 (up to 90 degrees Celsius) (IEC, 2023, 2025a). Rule 2 selects the cleaning interval τ^* that minimises LCOE in Equation (7), searched over 1 to 365 days. Rule 3 flags the degradation assumption as material if replacing the benchmark rate of 0.5 percent per year with the central rate raises LCOE by more than 5 percent. Table 8 lists the inputs and Table 9 the results.

Table 8. Inputs to the illustrative CRRSA application. Assumed values are illustrative; cited values come from the reviewed studies; hot-arid degradation inputs are comparator-derived assumptions, not measured Asian desert rates.

Parameter	Symbol (unit)	Hot-humid	Hot-arid	Basis
Hourly weather	G_h, T_a, v	Clear-sky peak 950 W/m2, monthly clearness 0.60 to 0.80; mean 29 C, daily swing 7 C; wind 0.5 to 2.5 m/s	Clear-sky peak 1,050 W/m2, clearness 0.85 to 0.90; mean 21 to 37 C, daily swing 14 C; wind 1.5 to 4.5 m/s	Assumed synthetic year
Annual insolation	H (kWh/m2)	1,789	2,570	Computed from hourly year
Faiman coefficients	U_0, U_1	25.0, 6.84 (open rack)	25.0, 6.84 (open rack)	Faiman (2008)
Temperature coefficient	γ (per C)	-0.0035	-0.0035	Assumed, near Limmanee et al. (2016) threshold
Degradation, benchmark	R_d (%/year)	0.5	0.5	Jordan et al. (2016)
Degradation, central	R_d (%/year)	1.42 (Indian hot zones, measured)	1.01 (assumed from Djibouti comparator)	Dubey et al. (2017); Daher et al. (2022)
Degradation, high	R_d (%/year)	1.90 (Thai upper bound, measured)	1.39 (assumed from Djibouti upper bound)	Limmanee et al. (2017); Daher et al. (2022)
Soiling rate	s (%/day)	0.0185	0.607	Li et al. (2024), 2% in 108 days; Hammad et al. (2018)
Costs and finance	C_0, O, c_k, r, N	650 USD/kW, 10 USD/kW/year, 0.10 USD/kW per clean, 7%, 25 years	Same	Assumed
Other losses	η_{BOS}	0.88	0.88	Assumed

Table 9. Results of the illustrative CRRSA application (open-rack T98 under Rule 1; optimal cleaning interval under Rule 2; LCOE change under Rule 3). Hot-arid rows are conditional on the transferred Djibouti degradation inputs.

Site and case	Degradation (%/year)	T98 and cleaning interval	25-year yield (MWh/kW)	LCOE (US cents/kWh) and change
Hot-humid, benchmark	0.50	51.8 C, no extension; 77 days	34.35	4.74 (reference)
Hot-humid, central	1.42	As above	30.87	5.12 (+7.93%)
Hot-humid, high	1.90	As above	29.24	5.32 (+12.17%)
Hot-arid, benchmark	0.50	61.1 C, no extension; 13 days	47.03	3.59 (reference)
Hot-arid, central (comparator-derived)	1.01	As above	44.31	3.74 (+4.36%)
Hot-arid, high (comparator-derived)	1.39	As above	42.41	3.86 (+7.66%)

The hourly thermal channel removes 6.7 percent of irradiance-weighted output at the hot-humid site and 8.1 percent at the hot-arid site, giving clean first-year yields of 1,469 and 2,079 kWh per kW. Under Rule 1, the open-rack T98 is 51.8 degrees Celsius at the hot-humid site and 61.1 degrees Celsius at the hot-arid site, so neither requires IEC TS 63126 testing when well ventilated; the effect of mounting is examined below. Under Rule 2, the low humid soiling rate gives an optimal interval of 77 days and a mean soiling ratio of 0.9929, while the arid site requires cleaning every 13 days at 2.81 US dollars per kW per year for a mean soiling ratio of 0.9605; a fixed 30-day schedule there would raise LCOE by 3.22 percent relative to the optimum. Under Rule 3, the measured central rate raises LCOE by 7.93 percent at the hot-humid site, which is material. At the hot-arid site the corresponding increase is 4.36 percent, below the threshold, and the high case (7.66 percent) crosses it; both results are conditional on degradation rates transferred from the Djibouti comparator, because no multi-site hot-arid Asian rate was located (Daher et al., 2022).

Equation (9) assumes linear accumulation and full recovery at each cleaning. Table 10 relaxes both assumptions with a daily simulation that matches the script used for every number reported here. The state variable is the accumulated fractional soiling loss L, starting from clean glass on 1 January. Each day is processed in four steps: (1) accumulation, L increases by s, capped at 0.9; (2) rain check, on a rain day L is multiplied by one minus the rain removal fraction, set to 1 so that rain fully cleans; (3) cleaning check, if the running day count since the start is a multiple of τ, L is multiplied by one minus the cleaning recovery fraction (1, 0.95 or 0.90) and one cleaning event is counted; (4) the end-of-day soiling ratio $1 - L$ is recorded. Residual soiling left by incomplete cleaning carries into the next day; rain removal is complete in this example, so no residual remains after a rain day. Rain occurs only at the hot-humid site, on every third day from day 151 (1 June) to day 271 (28 September), 41 days in total, as a stylised monsoon; the hot-arid site has no rain. The simulation runs for 12 years; the first is discarded as spin-up, and the mean soiling ratio and the number of cleanings per year, n_c, are averaged over the remaining 11, so cleaning dates that drift across years are averaged. The annual cleaning cost is $c_k n_c$ from Equation (11), entered as K_t in Equation (7). The cleaning interval is then optimised as under Rule 2.

Table 10. Sensitivity of the optimal cleaning interval, cleaning cost, soiling ratio and LCOE to cleaning recovery and monsoon rain (daily simulation, central degradation rate; changes relative to full recovery without rain at the same site; hot-arid rows use comparator-derived degradation).

Site and scenario	Optimal interval (days) and cleanings per year	Annual cleaning cost (USD/kW)	Mean soiling ratio	LCOE (US cents/kWh) and change
Hot-humid, full recovery, no rain	72; 5.00	0.50	0.9934	5.117 (reference)
Hot-humid, 95% recovery	72; 5.00	0.50	0.9927	5.120 (+0.07%)
Hot-humid, 90% recovery	72; 5.00	0.50	0.9920	5.124 (+0.15%)
Hot-humid, full recovery, monsoon rain	365; 1.00	0.10	0.9920	5.093 (-0.45%)
Hot-humid, 90% recovery, monsoon rain	365; 1.00	0.10	0.9912	5.097 (-0.38%)
Hot-arid, full recovery, no rain	13; 28.00	2.80	0.9636	3.729 (reference)
Hot-arid, 95% recovery	13; 28.00	2.80	0.9594	3.745 (+0.43%)
Hot-arid, 90% recovery	12; 30.45	3.045	0.9585	3.762 (+0.89%)

Incomplete recovery lowers the mean soiling ratio and raises LCOE by less than 1 percent at both sites; at the arid site 90 percent recovery shortens the optimal interval from 13 to 12 days. The monsoon rows need explicit reconciliation, because their mean soiling ratio (0.9920) is lower than in the no-rain reference (0.9934) yet LCOE falls. The cause is the optimiser's response to rain, not an error. Holding the reference interval of 72 days, rain raises the mean soiling ratio to 0.9960 and lowers LCOE by 0.26 percent. Because rain cleans the array for four months, however, the optimal interval lengthens to 365 days, so cleanings fall from five to one per year and annual cleaning cost from 0.50 to 0.10 US dollars per kW; soiling then accumulates through the longer dry season and the mean soiling ratio falls to 0.9920. Decomposing the move from the reference to the monsoon optimum, the cleaning-cost saving alone lowers LCOE by 0.60 percent and the energy loss alone raises it by 0.15 percent, giving the net fall of 0.45 percent. The optimiser accepts slightly dirtier modules in exchange for fewer paid cleanings, consistent with the global finding that cleaning has most value in high-soiling, low-rainfall regions (Mithhu et al., 2021).

Rule 1 depends on mounting. The Faiman coefficients describe heat loss from both module faces: U_0 captures radiative and natural-convective loss and U_1 the additional wind-driven convective loss (Faiman, 2008). Mounting a module close to a roof restricts rear-side airflow and reduces both terms; reviews of thermal correlations report parameters that depend on mounting configuration (Skoplaki & Palyvos, 2009) and which Kempe et al. (2024) represent through an effective standoff height. No verified source in this review gives scaling factors for Asian rooftops, so Table 11 applies assumed uniform reductions to both coefficients by factors of 0.75, 0.6 and 0.5 and recomputes T98 from the same hourly years.

Table 11. Sensitivity of T98 and the IEC TS 63126 level to reduced ventilation, represented by scaling both Faiman coefficients by an assumed factor (hourly synthetic years of Table 8).

Scaling factor	U_0, U_1	Hot-humid T98 and level	Hot-arid T98 and level
1.00 (open rack)	25.0, 6.84	51.8 C, no extension	61.1 C, no extension
0.75	18.75, 5.13	58.1 C, no extension	67.9 C, no extension
0.60	15.0, 4.10	64.6 C, no extension	74.5 C, Level 1
0.50	12.5, 3.42	71.1 C, Level 1	81.0 C, Level 2

The hot-arid site crosses the 70 degrees Celsius threshold at a scaling factor of 0.6 and reaches Level 2 at 0.5, whereas the hot-humid site needs Level 1 only at 0.5. High-temperature qualification therefore depends more on mounting than on climate family, consistent with the standoff analysis of Kempe et al. (2024). Taken together, under these assumptions the measured degradation rate dominates cost risk at the hot-humid site, while at the hot-arid site cleaning policy dominates and the degradation result remains conditional on the transferred comparator rates (Dubey et al., 2017; Daher et al., 2022; Mithhu et al., 2021).

9. Research agenda and evidence gaps

The evidence assembled here is uneven, and its weaknesses define the research agenda. First, long-term field data for TOPCon, HJT and bifacial glass-glass modules in hot-humid Asia are almost absent, even though these technologies now dominate supply; existing evidence is largely accelerated testing (Hacke et al., 2024; Pirot-Berson et al., 2024). Second, peer-reviewed multi-year degradation rates for Vietnam, Indonesia, the Philippines, Bangladesh and Malaysia were not located, and hot-arid Asian sites lack multi-site degradation studies comparable to the Indian surveys (Limmanee et al., 2017; Bayandelger et al., 2018). Third, methodological inconsistency undermines comparison; a common reporting protocol stating estimator, correction model, baseline, uncertainty, sample size and technology generation would make Asian rates comparable (Daher et al., 2022; Kumar & Kumar, 2017). Fourth, the interaction between soiling and degradation, including any effect of soiled, dew-wetted glass on PID leakage and the abrasion of coatings by cleaning, needs controlled field experiments, which would also allow the coupling terms omitted in Section 8.3 to be parameterised (Bomber et al., 2024). Fifth, a hot-humid qualification label analogous to the desert label is needed, built on Asian dew and salt profiles and on the UV-illuminated PID methods now in the specification (Lelièvre et al., 2022; IEC, 2025b). Sixth, water-scarce cleaning requires joint optimisation of water source, method and coating durability under Gulf and Thar conditions (Boeing et al., 2022; Mithhu et al., 2021). Two further gaps deserve mention. The UVID-browning trade-off in encapsulant selection has not been resolved for high-UV Asian deserts (Sinha et al., 2023), and the share of Asian rooftop arrays whose 98th percentile temperature exceeds the 70 degrees Celsius limit of the base standards is unknown (Kempe et al., 2024). Institutional arrangements matter as much as technical studies. The Indian national surveys demonstrate the value of repeated, methodologically consistent campaigns led by public research institutions (NCPRE & NISE, 2019), and comparable programmes in Southeast Asia and the Gulf would fill many of these gaps.

10. Conclusion

In the reviewed evidence, photovoltaic modules in Asia's hot climates do not consistently degrade at the global median rate that many project models assume, but neither do they degrade at a single higher rate. The two Indian national surveys, the strongest Asian datasets, found crystalline silicon degrading on average at roughly two to three times the global median, with hot zones, small systems and rooftop installations faring worst, and with system size and mounting associated with larger differences than climate zone. Tropical studies in Thailand and Singapore span outcomes from near-benchmark to severe within the same climate, and long-term rates from hot-arid Asian sites remain scarce. In the hot-humid tropics, potential-induced degradation, moisture-driven corrosion and discolouration dominate the field failures reviewed. In the Gulf, soiling dominates the short-term energy balance, with uncleaned arrays losing up to half their output within months and dew-driven cementation complicating water-scarce cleaning.

The newest module technologies change the risk profile rather than remove it. Ultraviolet-induced degradation, front-side polarisation in TOPCon, and sodium and moisture sensitivity in heterojunction designs have been demonstrated in accelerated laboratory tests, but multi-year field records in hot Asian climates are lacking. The current qualification standards screen design flaws and now include a potential-induced degradation test and a high-temperature specification, but they apply stresses singly and do not claim to predict field lifetime. A recomputed sensitivity shows that plausible changes in degradation and soiling assumptions raise levelised cost by about 11 to 14 percent.

The Climate-Resolved Reliability and Soiling Assessment framework treats climate as a stress vector, couples degradation, soiling and thermal losses, weights qualification to site stresses and feeds the results into a cost model with field feedback. Its illustrative application, which treats the loss channels as independent even though the omitted interactions could raise or lower combined loss, shows how measured degradation rates drive cost risk at a hot-humid site; at a hot-arid site cleaning policy dominates, and the degradation result is conditional on rates transferred from a non-Asian desert comparator. Mounting rather than climate family decides high-temperature qualification. The framework is proposed and has not been empirically validated; its coupling terms remain unparameterised, and its value depends on the field data, consistent reporting and climate-specific testing identified in the research agenda.

References

Abdallah, A. A., Abdelrahim, M., Elgaili, M., Pasha, M., Mroue, K., & Abutaha, A. (2024). Degradation of photovoltaic module backsheet materials in desert climate. *Solar Energy Materials and Solar Cells, 277*, Article 113118. https://doi.org/10.1016/j.solmat.2024.113118

Abdallah, A., Martinez, D., Figgis, B., & El Daif, O. (2016). Performance of silicon heterojunction photovoltaic modules in Qatar climatic conditions. *Renewable Energy, 97*, 860-865. https://doi.org/10.1016/j.renene.2016.06.044

Abdulla, H., Sleptchenko, A., & Nayfeh, A. (2024). Photovoltaic systems operation and maintenance: A review and future directions. *Renewable and Sustainable Energy Reviews, 195*, Article 114342. https://doi.org/10.1016/j.rser.2024.114342

Aghaei, M., Fairbrother, A., Gok, A., Ahmad, S., Kazim, S., Lobato, K., Oreski, G., Reinders, A., Schmitz, J., Theelen, M., Yilmaz, P., & Kettle, J. (2022). Review of degradation and failure phenomena in photovoltaic modules. *Renewable and Sustainable Energy Reviews, 159*, Article 112160. https://doi.org/10.1016/j.rser.2022.112160

Amin, N., Lung, C. W., & Sopian, K. (2009). A practical field study of various solar cells on their performance in Malaysia. *Renewable Energy, 34*(8), 1939-1946. https://doi.org/10.1016/j.renene.2008.12.005

Astete, I., Castro, M., Lorca, Á., & Negrete-Pincetic, M. (2024). Optimal cleaning scheduling for large photovoltaic portfolios. *Applied Energy, 372*, Article 123760. https://doi.org/10.1016/j.apenergy.2024.123760

Atta, S., Onyishi, E. E., & Appiah, S. A. (2024). Theoretical analysis of charge transport and recombination losses in thin film solar cell architectures. *International Journal of Engineering and Modern Technology, 10*(10), 147-170. https://doi.org/10.56201/ijemt.v10.no10.2024.pg147.170

Badran, G., & Dhimish, M. (2022). Field study on the severity of photovoltaic potential induced degradation. *Scientific Reports, 12*(1), Article 22094. https://doi.org/10.1038/s41598-022-26310-y

Bayandelger, B. E., Ueda, Y., Batbayar, B., Adiyabat, A., Enebish, N., & Otani, K. (2018). Long-term performance and degradation rate analyses of photovoltaic modules exposed in the Gobi Desert, Mongolia. *Japanese Journal of Applied Physics, 57*(8), Article 08RG07. https://doi.org/10.7567/JJAP.57.08RG07

Boeing, A., Neda, M., Steinberg, S., & Batista, J. (2022). The impact of lower quality water on soiling removal from photovoltaic panels. *Renewable and Sustainable Energy Reviews, 169*, Article 112870. https://doi.org/10.1016/j.rser.2022.112870

Bomber, J., Einhorn, A., Engtrakul, C., Lanaghan, C., Linger, J., Micheli, L., Miller, D. C., Morse, J., Moutinho, H., Muller, M., Newkirk, J. M., Simpson, L., To, B., Toth, S., Curtis, T., Li, F., Tamizhmani, G., Tatapudi, S., Alberts, V., . . . Hoffman, A. (2024). Soiling, cleaning, and abrasion: The results of the 5-year photovoltaic glass coating field study. *Solar Energy Materials and Solar Cells, 275*, Article 113035. https://doi.org/10.1016/j.solmat.2024.113035

Chen, J., Pan, G., Ouyang, J., Ma, J., Fu, L., & Zhang, L. (2020). Study on impacts of dust accumulation and rainfall on PV power reduction in East China. *Energy, 194*, Article 116915. https://doi.org/10.1016/j.energy.2020.116915

Cherupurakal, N., Mozumder, M. S., Mourad, A.-H. I., & Lalwani, S. (2021). Recent advances in superhydrophobic polymers for antireflective self-cleaning solar panels. *Renewable and Sustainable Energy Reviews, 151*, Article 111538. https://doi.org/10.1016/j.rser.2021.111538

Conceição, R., González-Aguilar, J., Merrouni, A. A., & Romero, M. (2022). Soiling effect in solar energy conversion systems: A review. *Renewable and Sustainable Energy Reviews, 162*, Article 112434. https://doi.org/10.1016/j.rser.2022.112434

Costa, S. C. S., Diniz, A. S. A. C., & Kazmerski, L. L. (2018). Solar energy dust and soiling R&D progress: Literature review update for 2016. *Renewable and Sustainable Energy Reviews, 82*, 2504-2536. https://doi.org/10.1016/j.rser.2017.09.015

Daher, D. H., Gaillard, L., & Ménézo, C. (2022). Experimental assessment of long-term performance degradation for a PV power plant operating in a desert maritime climate. *Renewable Energy, 187*, 44-55. https://doi.org/10.1016/j.renene.2022.01.056

de Oliveira, M. C. C., Diniz Cardoso, A. S. A., Viana, M. M., & Lins, V. F. C. (2018). The causes and effects of degradation of encapsulant ethylene vinyl acetate copolymer (EVA) in crystalline silicon photovoltaic modules: A review. *Renewable and Sustainable Energy Reviews, 81*, 2299-2317. https://doi.org/10.1016/j.rser.2017.06.039

Dehghan, M., Rashidi, S., & Waqas, A. (2022). Modeling of soiling losses in solar energy systems. *Sustainable Energy Technologies and Assessments, 53*, Article 102435. https://doi.org/10.1016/j.seta.2022.102435

Dhaouadi, R., Al-Othman, A., Aidan, A. A., Tawalbeh, M., & Zannerni, R. (2021). A characterization study for the properties of dust particles collected on photovoltaic (PV) panels in Sharjah, United Arab Emirates. *Renewable Energy, 171*, 133-140. https://doi.org/10.1016/j.renene.2021.02.083

Dubey, R., Chattopadhyay, S., Kuthanazhi, V., Kottantharayil, A., Solanki, C. S., Arora, B. M., Narasimhan, K. L., Vasi, J., Bora, B., Singh, Y. K., & Sastry, O. S. (2017). Comprehensive study of performance degradation of field-mounted photovoltaic modules in India. *Energy Science & Engineering, 5*(1), 51-64. https://doi.org/10.1002/ese3.150

Eder, G. C., Voronko, Y., Dimitriadis, S., Knöbl, K., Ujvári, G., Berger, K. A., Halwachs, M., Neumaier, L., & Hirschl, C. (2019). Climate specific accelerated ageing tests and evaluation of ageing induced electrical, physical, and chemical changes. *Progress in Photovoltaics: Research and Applications, 27*(11), 934-949. https://doi.org/10.1002/pip.3090

Faiman, D. (2008). Assessing the outdoor operating temperature of photovoltaic modules. *Progress in Photovoltaics: Research and Applications, 16*(4), 307-315. https://doi.org/10.1002/pip.813

Fares, E., Buffiere, M., Figgis, B., Haik, Y., & Isaifan, R. J. (2021). Soiling of photovoltaic panels in the Gulf Cooperation Council countries and mitigation strategies. *Solar Energy Materials and Solar Cells, 231*, Article 111303. https://doi.org/10.1016/j.solmat.2021.111303

Gideon, E. N., Adaramola, T. S., & Fadero, S. (2019). Reliability engineering and failure analysis in complex engineering systems. *Iconic Research and Engineering Journals, 2*(11), 703-727. https://doi.org/10.64388/IREV2I11-1722490

Hachicha, A. A., Al-Sawafta, I., & Said, Z. (2019). Impact of dust on the performance of solar photovoltaic (PV) systems under United Arab Emirates weather conditions. *Renewable Energy, 141*, 287-297. https://doi.org/10.1016/j.renene.2019.04.004

Hacke, P., Molto, C., Colvin, D., Smith, R., Mahmood, F. I., Li, F., Oh, J., Tamizhmani, G., & Seigneur, H. (2025). Polarization-type potential-induced degradation in bifacial PERC modules in the field. *EPJ Photovoltaics, 16*, Article 16. https://doi.org/10.1051/epjpv/2025004

Hacke, P., Spataru, S., Habersberger, B., & Chen, Y. (2024). Field-representative evaluation of PID-polarization in TOPCon PV modules by accelerated stress testing. *Progress in Photovoltaics: Research and Applications, 32*(5), 346-355. https://doi.org/10.1002/pip.3774

Hacke, P., Spataru, S., Terwilliger, K., Perrin, G., Kurtz, S., & Wohlgemuth, J. (2015). Accelerated testing and modeling of potential-induced degradation as a function of temperature and relative humidity. *IEEE Journal of Photovoltaics, 5*(6), 1549-1553. https://doi.org/10.1109/JPHOTOV.2015.2466463

Hammad, B., Al-Abed, M., Al-Ghandoor, A., Al-Sardeah, A., & Al-Bashir, A. (2018). Modeling and analysis of dust and temperature effects on photovoltaic systems' performance and optimal cleaning frequency: Jordan case study. *Renewable and Sustainable Energy Reviews, 82*, 2218-2234. https://doi.org/10.1016/j.rser.2017.08.070

He, B., Lu, H., Zheng, C., & Wang, Y. (2023). Characteristics and cleaning methods of dust deposition on solar photovoltaic modules: A review. *Energy, 263*, Article 126083. https://doi.org/10.1016/j.energy.2022.126083

Huang, X., Wang, H., Jiang, X., & Yang, H. (2023). Performance degradation and reliability evaluation of crystalline silicon photovoltaic modules without and with considering measurement reproducibility: A case study in desert area. *Renewable Energy, 219*, Article 119421. https://doi.org/10.1016/j.renene.2023.119421

Ilse, K. K., Figgis, B. W., Naumann, V., Hagendorf, C., & Bagdahn, J. (2018a). Fundamentals of soiling processes on photovoltaic modules. *Renewable and Sustainable Energy Reviews, 98*, 239-254. https://doi.org/10.1016/j.rser.2018.09.015

Ilse, K. K., Figgis, B. W., Werner, M., Naumann, V., Hagendorf, C., Pöllmann, H., & Bagdahn, J. (2018b). Comprehensive analysis of soiling and cementation processes on PV modules in Qatar. *Solar Energy Materials and Solar Cells, 186*, 309-323. https://doi.org/10.1016/j.solmat.2018.06.051

Ilse, K., Micheli, L., Figgis, B. W., Daßler, D., Hanifi, H., Wolfertstetter, F., Naumann, V., Hagendorf, C., Gottschalg, R., & Bagdahn, J. (2019). Techno-economic assessment of soiling losses and mitigation strategies for solar power generation. *Joule, 3*(10), 2303-2321. https://doi.org/10.1016/j.joule.2019.08.019

International Electrotechnical Commission. (2021). *Terrestrial photovoltaic (PV) modules: Design qualification and type approval. Part 2: Test procedures* (IEC 61215-2:2021, Ed. 2.0). IEC. https://webstore.iec.ch/en/publication/68602

International Electrotechnical Commission. (2023). *Photovoltaic (PV) module safety qualification. Part 1: Requirements for construction* (IEC 61730-1:2023, Ed. 3.0). IEC. https://webstore.iec.ch/en/publication/59803

International Electrotechnical Commission. (2025a). *Guidelines for qualifying PV modules, components and materials for operation at high temperatures* (IEC TS 63126:2025, Ed. 2.0). IEC. https://webstore.iec.ch/en/publication/110129

International Electrotechnical Commission. (2025b). *Photovoltaic (PV) modules: Test methods for the detection of potential-induced degradation. Part 1: Crystalline silicon* (IEC TS 62804-1:2025, Ed. 2.0). IEC. https://webstore.iec.ch/en/publication/71747

Jordan, D. C., & Kurtz, S. R. (2013). Photovoltaic degradation rates: An analytical review. *Progress in Photovoltaics: Research and Applications, 21*(1), 12-29. https://doi.org/10.1002/pip.1182

Jordan, D. C., Haegel, N., & Barnes, T. M. (2022). Photovoltaics module reliability for the terawatt age. *Progress in Energy, 4*(2), Article 022002. https://doi.org/10.1088/2516-1083/ac6111

Jordan, D. C., Kurtz, S. R., VanSant, K., & Newmiller, J. (2016). Compendium of photovoltaic degradation rates. *Progress in Photovoltaics: Research and Applications, 24*(7), 978-989. https://doi.org/10.1002/pip.2744

Jordan, D. C., Silverman, T. J., Wohlgemuth, J. H., Kurtz, S. R., & VanSant, K. T. (2017). Photovoltaic failure and degradation modes. *Progress in Photovoltaics: Research and Applications, 25*(4), 318-326. https://doi.org/10.1002/pip.2866

Kaiss, E.-C. A., & Hassan, N. M. (2024). Optimizing the cleaning frequency of solar photovoltaic (PV) systems using numerical analysis and empirical models. *Renewable Energy, 228*, Article 120691. https://doi.org/10.1016/j.renene.2024.120691

Kempe, M., Ovaitt, S., Springer, M., Brown, M., Jordan, D., Sekulic, W., O'Brien, C., Jaubert, J.-N., Yu, Y., Oh, J., Tamizhmani, G., & Li, B. (2024). Close roof-mounted system temperature estimation for compliance to IEC TS 63126. *Solar Energy Materials and Solar Cells, 275*, Article 112987. https://doi.org/10.1016/j.solmat.2024.112987

Kumar, M., & Kumar, A. (2017). Performance assessment and degradation analysis of solar photovoltaic technologies: A review. *Renewable and Sustainable Energy Reviews, 78*, 554-587. https://doi.org/10.1016/j.rser.2017.04.083

Lelièvre, J. F., Couderc, R., Pinochet, N., Sicot, L., Munoz, D., Kopecek, R., Ferrada, P., Marzo, A., Olivares, D., Valencia, F., & Urrejola, E. (2022). Desert label development for improved reliability and durability of photovoltaic modules in harsh desert conditions. *Solar Energy Materials and Solar Cells, 236*, Article 111508. https://doi.org/10.1016/j.solmat.2021.111508

Li, F., Yuan, Z., & Wu, W. (2024). Experimental investigation of soiling losses on photovoltaic in high-density urban environments. *Applied Energy, 369*, Article 123572. https://doi.org/10.1016/j.apenergy.2024.123572

Limmanee, A., Songtrai, S., Udomdachanut, N., Kaewniyompanit, S., Sato, Y., Nakaishi, M., Kittisontirak, S., Sriprapha, K., & Sakamoto, Y. (2017). Degradation analysis of photovoltaic modules under tropical climatic conditions and its impacts on LCOE. *Renewable Energy, 102*, 199-204. https://doi.org/10.1016/j.renene.2016.10.052

Limmanee, A., Udomdachanut, N., Songtrai, S., Kaewniyompanit, S., Sato, Y., Nakaishi, M., Kittisontirak, S., Sriprapha, K., & Sakamoto, Y. (2016). Field performance and degradation rates of different types of photovoltaic modules: A case study in Thailand. *Renewable Energy, 89*, 12-17. https://doi.org/10.1016/j.renene.2015.11.088

Luo, W., Clement, C. E., Khoo, Y. S., Wang, Y., Khaing, A. M., Reindl, T., Kumar, A., & Pravettoni, M. (2021). Photovoltaic module failures after 10 years of operation in the tropics. *Renewable Energy, 177*, 327-335. https://doi.org/10.1016/j.renene.2021.05.145

Luo, W., Khoo, Y. S., Hacke, P., Jordan, D., Zhao, L., Ramakrishna, S., Aberle, A. G., & Reindl, T. (2019). Analysis of the long-term performance degradation of crystalline silicon photovoltaic modules in tropical climates. *IEEE Journal of Photovoltaics, 9*(1), 266-271. https://doi.org/10.1109/JPHOTOV.2018.2877007

Luo, W., Khoo, Y. S., Hacke, P., Naumann, V., Lausch, D., Harvey, S. P., Singh, J. P., Chai, J., Wang, Y., Aberle, A. G., & Ramakrishna, S. (2017). Potential-induced degradation in photovoltaic modules: A critical review. *Energy & Environmental Science, 10*(1), 43-68. https://doi.org/10.1039/C6EE02271E

Lyu, Y., Fairbrother, A., Gong, M., Kim, J. H., Gu, X., Kempe, M., Julien, S., Wan, K.-T., Napoli, S., Hauser, A., O'Brien, G., Wang, Y., French, R., Bruckman, L., Ji, L., & Boyce, K. (2020). Impact of environmental variables on the degradation of photovoltaic components and perspectives for the reliability assessment methodology. *Solar Energy, 199*, 425-436. https://doi.org/10.1016/j.solener.2020.02.020

Maghami, M. R., Hizam, H., Gomes, C., Radzi, M. A., Rezadad, M. I., & Hajighorbani, S. (2016). Power loss due to soiling on solar panel: A review. *Renewable and Sustainable Energy Reviews, 59*, 1307-1316. https://doi.org/10.1016/j.rser.2016.01.044

Makhija, A. S., & Bohra, S. S. (2023). Performance and degradation analysis for different solar photovoltaic technologies under hot and humid environment: A review. *Progress in Energy, 5*(4), Article 042002. https://doi.org/10.1088/2516-1083/acfc92

Mehdi, M., Ammari, N., Alami Merrouni, A., El Gallassi, H., Dahmani, M., & Ghennioui, A. (2023). An experimental comparative analysis of different PV technologies performance including the influence of hot-arid climatic parameters: Toward a realistic yield assessment for desert locations. *Renewable Energy, 205*, 695-716. https://doi.org/10.1016/j.renene.2023.01.082

Mekhilef, S., Saidur, R., & Kamalisarvestani, M. (2012). Effect of dust, humidity and air velocity on efficiency of photovoltaic cells. *Renewable and Sustainable Energy Reviews, 16*(5), 2920-2925. https://doi.org/10.1016/j.rser.2012.02.012

Mithhu, M. M. H., Rima, T. A., & Khan, M. R. (2021). Global analysis of optimal cleaning cycle and profit of soiling affected solar panels. *Applied Energy, 285*, Article 116436. https://doi.org/10.1016/j.apenergy.2021.116436

Nam, W., Choi, J., Kim, G., Hyun, J., Ahn, H., & Park, N. (2025). Predicting photovoltaic module lifespan based on combined stress tests and latent heat analysis. *Energies, 18*(2), Article 304. https://doi.org/10.3390/en18020304

National Centre for Photovoltaic Research and Education, & National Institute of Solar Energy. (2019). *All-India survey of photovoltaic module reliability: 2018*. Indian Institute of Technology Bombay and National Institute of Solar Energy. https://nise.res.in/upload/All-India-Survey-of-Photovoltaic-Module-Reliability_2018_Report.pdf

Owen-Bellini, M., Hacke, P., Miller, D. C., Kempe, M. D., Spataru, S., Tanahashi, T., Mitterhofer, S., Jankovec, M., & Topič, M. (2021). Advancing reliability assessments of photovoltaic modules and materials using combined-accelerated stress testing. *Progress in Photovoltaics: Research and Applications, 29*(1), 64-82. https://doi.org/10.1002/pip.3342

Pan, A., Lu, H., & Zhang, L.-Z. (2019). Experimental investigation of dust deposition reduction on solar cell covering glass by different self-cleaning coatings. *Energy, 181*, 645-653. https://doi.org/10.1016/j.energy.2019.05.223

Peinado Gonzalo, A., Pliego Marugán, A., & García Márquez, F. P. (2020). Survey of maintenance management for photovoltaic power systems. *Renewable and Sustainable Energy Reviews, 134*, Article 110347. https://doi.org/10.1016/j.rser.2020.110347

Pirot-Berson, L., Couderc, R., Bodeux, R., & Dupuis, J. (2024). Failure modes of silicon heterojunction photovoltaic modules in damp heat environment: Sodium and moisture effects. *Solar Energy Materials and Solar Cells, 278*, Article 113190. https://doi.org/10.1016/j.solmat.2024.113190

Segbefia, O. K., Akhtar, N., & Sætre, T. O. (2023). Moisture induced degradation in field-aged multicrystalline silicon photovoltaic modules. *Solar Energy Materials and Solar Cells, 258*, Article 112407. https://doi.org/10.1016/j.solmat.2023.112407

Segbefia, O. K., Imenes, A. G., & Sætre, T. O. (2021). Moisture ingress in photovoltaic modules: A review. *Solar Energy, 224*, 889-906. https://doi.org/10.1016/j.solener.2021.06.055

Singh, R., Sharma, M., & Yadav, K. (2022). Degradation and reliability analysis of photovoltaic modules after operating for 12 years: A case study with comparisons. *Renewable Energy, 196*, 1170-1186. https://doi.org/10.1016/j.renene.2022.07.048

Sinha, A., Qian, J., Moffitt, S. L., Hurst, K., Terwilliger, K., Miller, D. C., Schelhas, L. T., & Hacke, P. (2023). UV-induced degradation of high-efficiency silicon PV modules with different cell architectures. *Progress in Photovoltaics: Research and Applications, 31*(1), 36-51. https://doi.org/10.1002/pip.3606

Skoplaki, E., & Palyvos, J. A. (2009). On the temperature dependence of photovoltaic module electrical performance: A review of efficiency/power correlations. *Solar Energy, 83*(5), 614-624. https://doi.org/10.1016/j.solener.2008.10.008

Song, Z., Liu, J., & Yang, H. (2021). Air pollution and soiling implications for solar photovoltaic power generation: A comprehensive review. *Applied Energy, 298*, Article 117247. https://doi.org/10.1016/j.apenergy.2021.117247

Straub-Mück, M., Geyer-Klingeberg, J., & Rathgeber, A. W. (2025). Determinants of the long-term degradation rate of photovoltaic modules: A meta-analysis. *Renewable and Sustainable Energy Reviews, 216*, Article 115697. https://doi.org/10.1016/j.rser.2025.115697

Theristis, M., Stein, J. S., Deline, C., Jordan, D., Robinson, C. D., Sekulic, W., Anderberg, A., Colvin, D. J., Walters, J., Seigneur, H., & King, B. H. (2023). Onymous early-life performance degradation analysis of recent photovoltaic module technologies. *Progress in Photovoltaics: Research and Applications, 31*(2), 149-160. https://doi.org/10.1002/pip.3615

Touati, F., Chowdhury, N. A., Benhmed, K., San Pedro Gonzales, A. J. R., Al-Hitmi, M. A., Benammar, M., Gastli, A., & Ben-Brahim, L. (2017). Long-term performance analysis and power prediction of PV technology in the State of Qatar. *Renewable Energy, 113*, 952-965. https://doi.org/10.1016/j.renene.2017.06.078

Ullah, A., Imran, H., Maqsood, Z., & Butt, N. Z. (2019). Investigation of optimal tilt angles and effects of soiling on PV energy production in Pakistan. *Renewable Energy, 139*, 830-843. https://doi.org/10.1016/j.renene.2019.02.114

Yang, L., Hu, Z., He, Q., Liu, Z., Zeng, Y., Yang, L., Yu, X., & Yang, D. (2024). Insights into mechanism of UV-induced degradation in silicon heterojunction solar cells. *Solar Energy Materials and Solar Cells, 275*, Article 113022. https://doi.org/10.1016/j.solmat.2024.113022

Yeo, Z. Y., Ling, Z. P., Ho, J. W., Lim, Q. X., So, Y. H., & Wang, S. (2022). Status review and future perspectives on mitigating light-induced degradation on silicon-based solar cells. *Renewable and Sustainable Energy Reviews, 159*, Article 112223. https://doi.org/10.1016/j.rser.2022.112223

Yilmaz, P., Schmitz, J., & Theelen, M. (2022). Potential induced degradation of CIGS PV systems: A literature review. *Renewable and Sustainable Energy Reviews, 154*, Article 111819. https://doi.org/10.1016/j.rser.2021.111819

Zeedan, A., Barakeh, A., Al-Fakhroo, K., Touati, F., & Gonzales, A. S. P. (2021). Quantification of PV power and economic losses due to soiling in Qatar. *Sustainability, 13*(6), Article 3364. https://doi.org/10.3390/su13063364